SCIENTIFIC REPORTS

OPEN

Glucanocellulosic ethanol: the undiscovered biofuel potential in energy crops and marine biomass

Received: 27 March 2015
Accepted: 27 July 2015
Published: 01 September 2015

Christian Falter[1,*], Claudia Zwikowics[1,*], Dennis Eggert[2,3], Antje Blümke[1], Marcel Naumann[1], Kerstin Wolff[1], Dorothea Ellinger[1], Rudolph Reimer[2] & Christian A. Voigt[1]

Converting biomass to biofuels is a key strategy in substituting fossil fuels to mitigate climate change. Conventional strategies to convert lignocellulosic biomass to ethanol address the fermentation of cellulose-derived glucose. Here we used super-resolution fluorescence microscopy to uncover the nanoscale structure of cell walls in the energy crops maize and Miscanthus where the typical polymer cellulose forms an unconventional layered architecture with the atypical (1, 3)-β-glucan polymer callose. This raised the question about an unused potential of (1, 3)-β-glucan in the fermentation of lignocellulosic biomass. Engineering biomass conversion for optimized (1, 3)-β-glucan utilization, we increased the ethanol yield from both energy crops. The generation of transgenic Miscanthus lines with an elevated (1, 3)-β-glucan content further increased ethanol yield providing a new strategy in energy crop breeding. Applying the (1, 3)-β-glucan-optimized conversion method on marine biomass from brown macroalgae with a naturally high (1, 3)-β-glucan content, we not only substantially increased ethanol yield but also demonstrated an effective co-fermentation of plant and marine biomass. This opens new perspectives in combining different kinds of feedstock for sustainable and efficient biofuel production, especially in coastal regions.

An increasing worldwide demand for energy combined with decreasing fossil energy resources not only fosters climate change[1] but also explorations for fossil energy in sensitive ecosystems[2]. A key strategy to mitigate climate change is to substitute fossil by renewable energy sources. Because liquid fuels play a predominant role in the transportation sector, second generation biofuels from lignocellulosic feedstock reveal a high potential in substituting fossil fuels[3]. Restrictions in the production of ethanol from biomass mainly derive from the plant cell wall's recalcitrance, which is primarily determined by cellulose crystallinity but also lignin and hemicellulose content[4,5].

To improve second generation ethanol production, we tried to identify and increase the content of cell wall polymers that are easily degradable and contain readily fermentable residues. Hence, polymers that only consist of glucose would represent an optimal substrate for ethanol fermentation with efficient microorganisms like yeast (*Saccharomyces cerevisiae*). Apart from the major (1, 4)-β-glucan cell wall polymer cellulose[6], only two other cell wall polymers consist entirely of glucose: (1, 3)-β-glucan, known as callose in plants[7], and (1, 3;1, 4)-β-glucan, a mixed-linkage glucan found in plants of the order Poales, in horsetail (*Equisetum* spp.), and in bryophytes[8]. (1, 3)-β-glucan is important to maintain the vascular system, for pollen development, and cell plate formation in growing tissue as well as for defense responses[7]. Mixed-linkage glucan can serve as an energy storage and has a growth-related function in vegetative tissues of grasses[9]. Because of their biological function, the abundance of these β-glucan polymers has been considered low in lignocellulosic biomass[10]. Therefore, these polymers have not been targeted to

[1]Phytopathology and Biochemistry, Biocenter Klein Flottbek, University of Hamburg, Hamburg, Germany. [2]Heinrich Pette Institute, Leibniz Institute for Experimental Virology, Hamburg, Germany. [3]Max Planck Institute for the Structure and Dynamics of Matter, Hamburg, Germany. *These authors contributed equally to this work. Correspondence and requests for materials should be addressed to C.A.V. (email: christian.voigt@uni-hamburg.de)

improve saccharification. To test whether an undiscovered potential of β-glucan processing to ethanol would exist, we determine the (1, 3)-β-glucan and (1, 3;1, 4)-β-glucan content in lignocellulosic biomass of crops representing a major source of lignocellulosic feedstock from agriculture in temperate climates: barley (*Hordeum vulgare*), wheat (*Triticum aestivum*), and maize (*Zea mays*); as well as in the model plants Arabidopsis (*Arabidopsis thaliana*) and Brachypodium (*Brachypodium distachyon*), and the emerging, perennial grass Miscanthus (*Miscanthus* x *giganteus*). This low-input energy crop with high biomass yields in temperate climates has been proposed for sustainable lignocellulosic feedstock production[11].

Whereas the (1, 3;1, 4)-β-glucan content was relatively low in all tested plant species (0.2–0.5%), the (1, 3)-β-glucan content was exceptionally high in maize and Miscanthus, reaching 2% and 5% of total dry leaf biomass, respectively (Fig. 1a). The specificity of the florescent dye aniline blue for staining (1, 3)-β-glucan rather than (1, 3;1, 4)-β-glucan allowed its usage in assays for (1, 3)-β-glucan quantification and microscopic localization (Supplementary Fig. 1). Confocal laser scanning microscopy (CLSM) revealed an unexpectedly high (1, 3)-β-content in epidermal leaf cells of maize and Miscanthus (Fig. 1b), which we did not observe in the other examined plant species (Supplementary Fig. 2). Moreover, localization microscopy (LM), which we recently established for super-resolution analysis of β-glucan polymer networks in plant cells[12], facilitated three-dimensional rendering of (1, 3)-β-glucan and (1, 4)-β-glucan macrofibrils in cell walls (Fig. 1b). This microscopic technique revealed a parallel orientation of β-glucan polymer layers. The generation of videos based on three-dimensional rendered glucan macrofibrils data specifically addressed the visualization of direct interactions between the two cell wall polymers. Whereas in maize, interaction between (1, 3)-β-glucan and (1, 4)-β-glucan was mainly based on direct macrofibrils attachment (Supplementary Video 1), (1, 3)-β-glucan macrofibrils additionally partially surrounded (1, 4)-β-glucan macrofibrils in Miscanthus (Supplementary Video 2). This suggests the establishment of a tight polymer network that we also identified in epidermal leaf cells of Arabidopsis at sites of attempted pathogen penetration[12]. Our results from maize and Miscanthus provide first evidence that (1, 3)-β-glucan can be a major polymer of unchallenged secondary cell walls outside the vascular tissue. Interestingly, we also found a relatively high resistance of (1, 3)-β-glucan to chemical degradation by diluted trifluoroacetic and sulfuric acid (Supplementary Fig. 3), which supported the idea of an independent cell wall component rather than being part of the hemicellulose fraction[10].

Before engineering an improved utilization of (1, 3)-β-glucan-enriched biomass, we developed an equation to estimate the increase in biomass saccharification after optimized (1, 3)-β-glucan hydrolysis:

$$f(S)_i = \frac{A(P_x) \cdot \left(f(S)_{P_x} - f(S)_B\right)}{f(S)_B} + 1 \quad (1)$$

where $A(P_x)$ describes the relative amount of the glucan polymer P_x, $f(s)$ the glucose saccharification factor of the biomass B before optimization and of the glucan polymer P_x after optimized hydrolysis, and $f(s)_i$the increase in glucose saccharification after optimization. Based on equation (1), we expected an improved saccharification only if $f(s)_{Px} > f(s)_B$.

We analyzed the maize leaf biomass broth after dilute-sulfuric acid pretreatment, hydrolysis with the cell wall-degrading enzyme cocktail Accellerase 1500, and subsequent fermentation with a non-adapted, laboratory yeast strain. Here, we detected relative high contents of laminaribiose and –triose (Fig. 2a), which we distinguished from putative glucotrioses deriving from possible (1, 3;1, 4)-β-glucan degradation using a refractive index detector coupled to an HPLC-system (Supplementary Fig. 4). Due to their chemical composition and their relatively small size, we considered these (1, 3)-β-glucan degradation products as a potential, unused glucose source for fermentation. Therefore, we initiated experiments for optimizing (1, 3)-β-glucan hydrolysis and usage of (1, 3)-β-glucan degradation products for ethanol production. In a first step, we changed the yeast strain during fermentation to increase laminaribiose and –triose utilization during fermentation. The application of the yeast strain CEN.PK113-13D (CEN) that has been used to develop strains for optimized biomass fermentation[13] significantly improved laminaribiose utilization during fermentation, but did not effected laminaritriose utilization (Fig. 2a). The heterologous expression of the bacterial laminaribiose ABC transporter (LBT) from *Clostridium thermocellum*[14] in the yeast strain CEN (Supplementary Fig. 5a,b) further improved the laminaribiose and laminaritriose utilization (Fig. 2b), resulting in only residual amounts of laminaribiose and –triose in the fermentation broth (Fig. 2a). However, the utilization of laminaritetraose, long-chained (1, 3)-β-glucan, or oligomers deriving from (1, 4)-β-glucan and (1, 3;1, 4)-β-glucan hydrolysis was not facilitated (Supplementary Fig. 5c). Because of the efficient utilization of these two (1, 3)-β-glucan oligomers by CEN+LBT, we considered laminaribiose and –triose as direct contributors to the overall glucose saccharification. Hence, the generation of this yeast strain represented a decisive step in engineering optimized (1, 3)-β-glucan utilization from β-glucan-enriched biomass.

To further improve saccharification of (1, 3)-β-glucan-rich biomass, we initially screened 38 (1, 3)-β-glucanases from bacteria, fungi, and plants (Supplementary Table 1) that we heterologously expressed and purified from *Escherichia coli*. Six (1, 3)-β-glucanases showed a higher efficiency in (1, 3)-β-glucan hydrolysis than the Accellerase enzyme cocktail and a commercially available (1, 3)-β-glucanase from *Trichoderma reesei*, a well-studied and widely used fungus in second generation biofuel production[15] (Supplementary Fig. 6a). After confirming expression of these six (1, 3)-β-glucanases in *E. coli* (Supplementary Fig. 7), we determined their optimal pH and temperature range for enzymatic

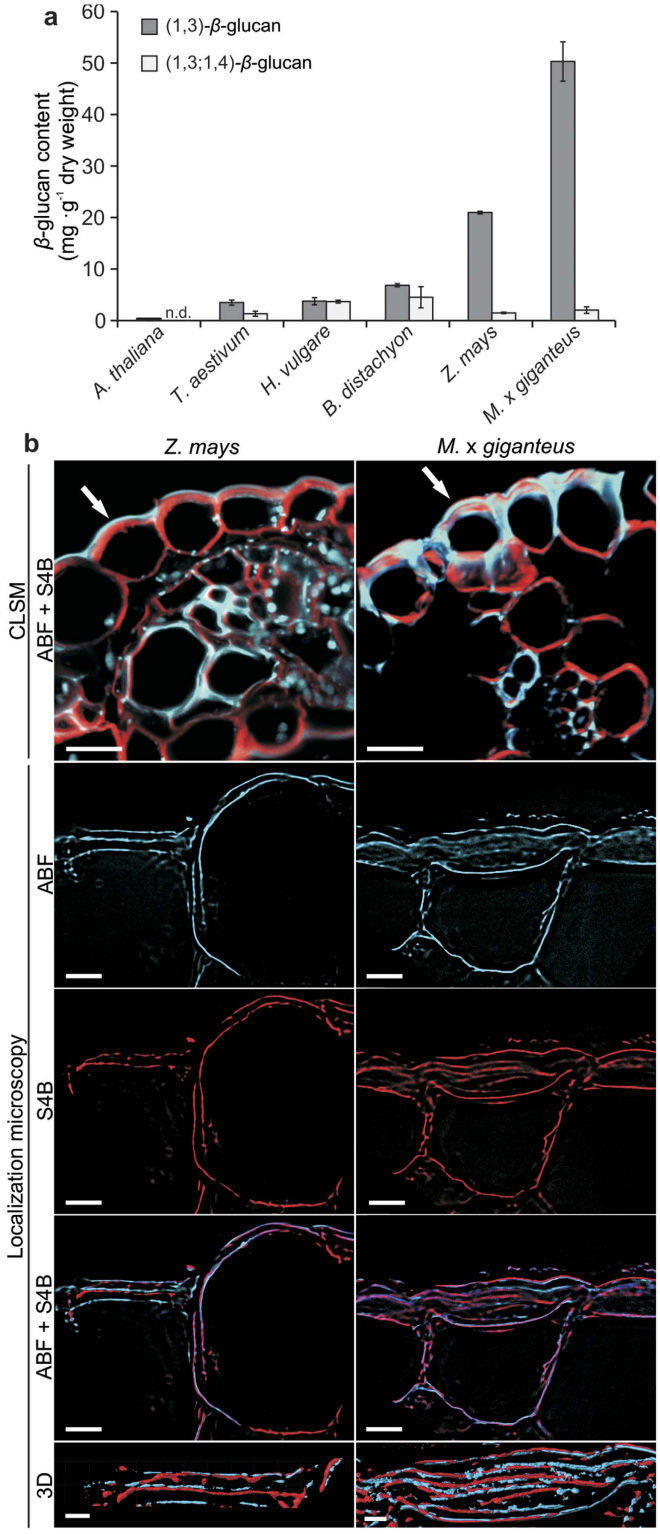

Figure 1. Layered cell wall architecture in maize and Miscanthus. (**a**) β-Glucan content in senesced leaf biomass. n.d., not detectable. Values represent the mean of three independent biological experiments. Error bars represent ± SE. (**b**) Confocal laser-scanning microscopy (CLSM) of aniline blue fluorochrome (ABF)-stained (1, 3)-β-glucan (blue channel) and pontamine fast scarlet 4B (S4B)-stained (1, 4)-β-glucan (red channel) cross sections of leaves from maize (*Z. mays*) amd Miscanthus (*M.* x *giganteus*). White arrows indicate epidermal cells with a high (1, 3)-β-glucan content and sites of localization microscopy (LM) application. 3D, surface rendering of β-glucan networks. Scale bars: CLSM, 50 μm; LM ABF/S4B, 5 μm; LM 3D, 2 μm.

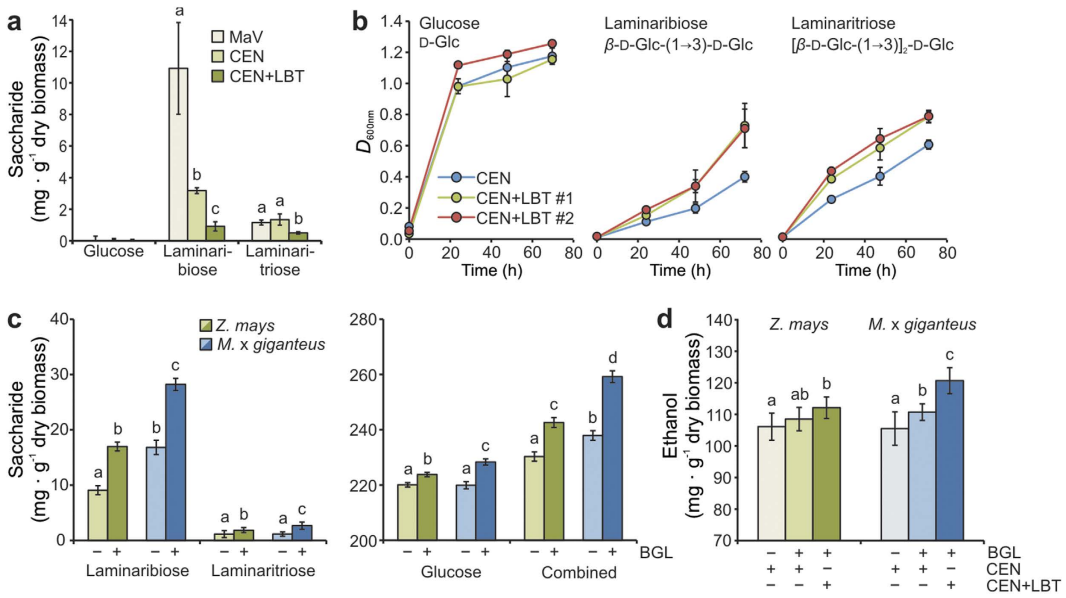

Figure 2. Engineered saccharification and ethanol production of (1, 3)-β-glucan-rich biomass. (**a**) Amounts of glucose and the oligosaccharides laminaribiose and –triose remaining in the fermentation broth after 48 h of maize leaf biomass fermentation comparing yeast strains MaV (non-adapted), CEN (adapted), and CEN+LBT (engineered). (**b**) *In vitro* growth assays of yeast strains CEN and CEN+LBT on substrates as indicated. (**c**) Amounts of laminaribiose and –triose (left panel) as well as glucose and the combined amount of these three (1, 3)-β-glucan hydrolysis products (right panel) as indicators for changes in saccharification efficiency of maize and Miscanthus leaf biomass due to additional *F. johnsoniae* (1, 3)-β-glucanase application (−/+ BGL) after standard biomass pretreatment. (**d**) Ethanol production after 48 h of fermentation using yeast strains CEN and CEN+LBT and −/+ BGL. Values represent the mean of three independent biological experiments. Letters a, b, c: groups with significant difference, $P < 0.05$ based on Tukey's test. Error bars represent ± SE.

activity (Supplementary Fig. 8). Under optimal conditions for each enzyme, we identified highest (1, 3)-β-glucanase activity for the enzyme from *Flavobacterium johnsoniae* (Supplementary Table 1), which was 3.3-times higher than the enzymatic activity of the commercially available (1, 3)-β-glucanase from *T. reesei*, resulting in an almost 70% hydrolyzing efficiency (Supplementary Fig. 9a). Combining the saccharification efficiency from non-optimized biomass processing (Fig. 2a) and the (1, 3)-β-glucan content of maize and Miscanthus biomass (Fig. 1a), we predicted a 4.0% increase in saccharification efficiency for maize and a 9.3% increase for Miscanthus using equation (1). The experimental data only slightly deviated from our prediction showing a 5.3% increase for maize and a 9.0% increase for Miscanthus (Fig. 2c). The improved second generation ethanol production reflected the efficiency of engineered (1, 3)-β-glucan processing due to i) optimization of its enzymatic hydrolysis and ii) enhanced utilization of its degradation products by the engineered yeast strain CEN+LBT, resulting in an increased ethanol production of 5.7% for maize and 14.4% for Miscanthus (Fig. 2d).

Our results from saccharification and fermentation of maize and Miscanthus biomass revealed a direct correlation between the (1, 3)-β-glucan content of the feedstock and an increased ethanol yield. Hence, we concluded that a further (1, 3)-β-glucan enrichment in biomass would result in increased ethanol yields. To test this hypothesis, we followed two strategies: i) increasing the (1, 3)-β-glucan content in potential feedstock for sustainable biomass production using a biotechnological approach; and ii) identifying new sources of (1, 3)-β-glucan-enriched biomass that could be used in our adapted fermentation process.

To increase the (1, 3)-β-glucan content in feedstock for sustainable biomass production, we overexpressed the GFP-tagged (1, 3)-β-glucan synthase gene *PMR4* (*POWDERY MILDEW RESISTANT4*) from Arabidopsis in Miscanthus (line *35S:PMR4-GFP*). *PMR4* overexpression in Arabidopsis increased (1, 3)-β-glucan content at infection sites but not in unchallenged tissue[16]. In contrast, we observed a constitutive increase in (1, 3)-β-glucan content in *35S:PMR4-GFP* Miscanthus lines, which was proportional to the relative *PMR4* expression level and reached a maximum of 8.5% in leaf tissue (Supplementary Fig. 10a,b). This result suggests different regulatory mechanisms of (1, 3)-β-glucan biosynthesis in Miscanthus and Arabidopsis, which would also explain the strong differences in their overall (1, 3)-β-glucan content (Fig. 1). As expected from Arabidopsis[16], PMR4-GFP was localized at the plasma membrane whereas single GFP of a transgenic Miscanthus control line was detectable in cytosolic strands (Supplementary Fig. 10c). We predicted an increase in saccharification efficiency of about 16% in the *35S:PMR4-GFP* line

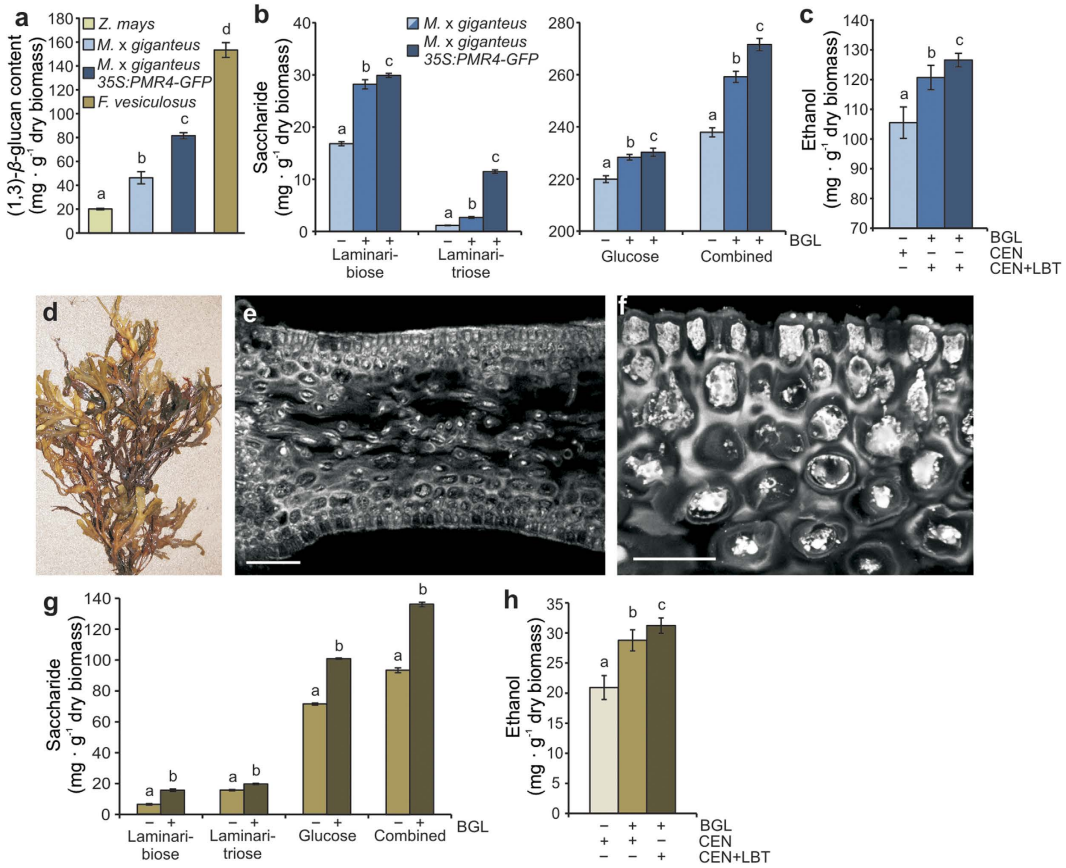

Figure 3. Enhanced saccharification and ethanol production in (1, 3)-β-glucan-enriched Miscanthus and marine biomass. (**a**) (1, 3)-β-glucan content in engineered Miscanthus leaf (*35S:PMR4-GFP*) and bladderwrack (*F. vesiculosus*) biomass. (**b**) Amounts of the oligosaccharides laminaribiose and –triose (left panel) as well as glucose and the combined amount of these three (1, 3)-β-glucan hydrolysis products (right panel) as indicators for changes in saccharification efficiency of Miscanthus wild-type and engineered leaf biomass due to additional *F. johnsoniae* (1, 3)-β-glucanase application (−/+ BGL) after standard biomass pretreatment. (**c**) Ethanol production after 48 h of fermentation using yeast strains CEN (adapted) and CEN+LBT (engineered) and −/+ BGL. (**d**) Thallus morphology of bladderwrack. Photo courtesy of Christian A. Voigt. (**e**) Micrograph showing cross section of the bladderwrack's blade after aniline blue fluorochrome-staining of (1, 3)-β-glucan. Micrograph taken by confocal laser-scanning microscopy. Scale bar, 100 μm. (**f**) Magnification of the blade's epidermal and cortex cells as indicated in (e). Scale bar = 20 μm. (**g**) Amounts of laminaribiose, –triose,glucose, and the combined amount of these three (1, 3)-β-glucan hydrolysis products as indicators for changes in saccharification efficiency of bladderwrack biomass −/+ BGL. (**h**) Ethanol production after 48 h of fermentation using the yeast strains CEN and CEN+LBT and −/+ BGL. Values represent the mean of three independent biological experiments. Letters a, b, c: groups with significant difference, $P < 0.05$ based on Tukey's test. Error bars represent ± SE.

with the highest (1, 3)-β-glucan content of 8.5% after optimized hydrolysis, which was relatively close to our experimental results showing a saccharification increase of 14.5%. (Fig. 3b). The improved saccharification of this Miscanthus line resulted in an increase in ethanol production of 20% compared to non-optimized Miscanthus wild-type biomass processing (Fig. 3c). These results revealed a previously undiscovered potential in the layered architecture of maize and Miscanthus leaf cell walls that contain an atypically high content of (1, 3)-β-glucan, which was unleashed by engineering optimized enzymatic hydrolysis and yeast fermentation. Moreover, (1, 3)-β-glucan enrichment represents a new target in breeding energy crops for improved second generation ethanol production.

In our second approach to identify new sources of (1, 3)-β-glucan-enriched biomass, we considered brown macroalgae with a naturally high (1, 3)-β-glucan content as a putative source. To examine the potential of (1, 3)-β-glucan utilization for ethanol production from this marine feedstock, we collected thalli of the brown macroalgae bladderwrack (*Fucus vesiculosus*) from the German Baltic Sea shore at Eckernförde near Hamburg (Fig. 3d). We determined an astonishing (1, 3)-β-glucan content of 15.3% (Fig. 3a) confirming previous studies of this macroalga[17]. CLSM revealed (1, 3)-β-glucan deposition in all tissues of the blade (Fig. 3e). However, highest (1, 3)-β-glucan accumulation occurred within

epidermal and cortex cells (Fig. 3f). The generation of three-dimensional videos from (1, 3)-β-glucan accumulation within the bladderwrack tissue allowed us to distinguish between different deposition patterns. Whereas elongated cells of the central pith region revealed a scattered (1, 3)-β-glucan deposition pattern (Supplementary Video 3), a relatively compact layer of (1, 3)-β-glucan was intracellular deposited in cortex and especially epidermal cells (Supplementary Video 4). Based on our previous results, we hypothesized that the optimized processing of (1, 3)-β-glucan-enriched bladderwrack biomass would result in increased ethanol production. We first tested the six (1, 3)-β-glucanases with highest activity on brown algae-derived (1, 3)-β-glucan as substrate. Similar to our previous test, the enzyme from *F. johnsoniae* showed highest activity with a hydrolyzing efficiency of 37.5% (Supplementary Fig. 9b). Using this (1, 3)-β-glucanase in addition to the Accellerase enzyme cocktail for biomass hydrolysis after dilute-sulfuric acid pretreatment, we increased bladderwrack biomass saccharification by 45.6% (Fig. 3g), which was close to the prediction of 46.4% using equation (1). Consequently, the ethanol yield was 50.5% higher in optimized CEN+LBT-driven fermentation compared to non-optimized (1, 3)-β-glucan processing (Fig. 3h).

Similar to Miscanthus, brown macroalgae have been considered for sustainable biomass production[18], however, without competing for arable land and food production. Because we demonstrated optimized ethanol production for both, (1, 3)-β-glucan-enriched plant and marine feedstock, we proposed our engineered biomass processing for co-fermentation of Miscanthus and bladderwrack biomass (Fig. 4a). A successful co-fermentation using equal amounts of Miscanthus and bladderwrack biomass proved the applicability of this engineered production approach (Fig. 4b). Regarding saccharification of mixed Miscanthus and bladderwrack biomass, we identified enzymatic hydrolysis as a field of further improvement. Here, the release of laminaribiose from (1, 3)-β-glucan was specifically inhibited during mixed Miscanthus and bladderwrack biomass processing compared to single biomass processing whereas inhibition did not occur for laminaritriose or glucose release in the mixed biomass approach (Fig. 4b).

Because brown macroalgae do not contain lignin and (1, 3)-β-glucan substantially contributed to improve second generation ethanol production in our study, we considered the produced ethanol as glucanocellulosic.

The effective co-fermentation opens new perspectives for sustainable and efficient ethanol production in bio-refineries, especially in coastal regions that combine the potential of offshore macroalgae aquaculture and proximate energy crop cultivation. An example for a coastal region that would fulfill these prerequisites is Schleswig-Holstein in northern Germany. Existing and planned offshore wind parks in the North and Baltic Sea would facilitate effective macroalgae aquacultures[19], and a high potential for Miscanthus cultivation in Schleswig-Holstein was shown in our recent study[20]. Hence, these coastal regions would represent prototypic sites for future biorefineries for plant and marine biomass co-fermentation, combining short delivery distances of feedstock with a high abundance of renewable electricity for processing, which could help to promote large-scale energy transition projects like the ambitious German *Energiewende*[21].

Methods

Biological material. Brachypodium (*Brachypodium distachyon*, inbred line Bd 21[22]), barley (*Hordeum vulgare*, cultivar Golden Promise[23]), wheat (*Triticum aestivum*, cultivar Nandu, Lochow-Petkus, Bergen-Wohlde, Germany), maize (*Zea mays*, inbred line A188[24]), and Miscanthus (*Miscanthus x giganteus*) were cultivated as described in Meineke *et al.*[25]. Arabidopsis (*Arabidopsis thaliana*, wild-type Columbia) was cultivated as described in Stein *et al.*[26]. Naturally dried leaf material was harvested manually at its final developmental stage after senescence and 2 additional weeks of drying[25]. Biomass was additionally dried at 50 °C for 2 days in a drying oven. Washed ashore thalli of the brown macroalga bladderwrack (*Fucus vesiculosus*) were collected in November from the Baltic Sea shore at Eckernförde (Schleswig-Holstein, Germany, geographical position: 54°27'57.5″N 9°50'28.0″E) and dried at 50 °C for 3 days. Plant and alga biomass was homogenized with a mill fitted with a 0.5 mm mesh screen prior processing. Material subject to (1, 3)-β-glucan extraction was ground in liquid nitrogen using a mortar and pestle.

(1, 3)-β-Glucan extraction and determination. 20 mg of mortared and lyophilized leaf or alga biomass was destained in ethanol (96%) at 50 °C and 600 rpm for 10 min. Subsequent procedures of (1, 3)-β-glucan determination followed the description in Voigt *et al.*[27]. Ethanol was removed after centrifugation (2 min, 10,000 g), and the sample was dried using a centrifugal evaporator. After a washing step with H_2O, the sample was dried again in a centrifugal evaporator. For (1, 3)-β-glucan extraction, the sample was resuspended in 400 µl of 1 M NaOH and incubated at 80 °C and 600 rpm for 1 h. After centrifugation (10 min, 2000 g), the supernatant was used for the aniline blue fluorescence assay for (1, 3)-β-glucan determination. 5 µl sample were mixed with 45 ml H_2O, 5 µl HCl (1 M), 220 µl K_2HPO_4 (150 mM), and 5 µl aniline blue fluorochrome (ABF, 0.1 mg·ml^{-1} in H_2O, Biosupplies, Australia). Standards ranging from 0 to 20 µg ml^{-1} were generated from purified (1, 3)-β-glucan from *Euglena gracilis* (Sigma-Aldrich, Germany) in the same way as described for plant and alga samples. Additional standards were generated accordingly from oat and barley (1, 3;1, 4)-β-glucan deriving from the mixed-linkage beta-glucan kit (Megazyme, Ireland) to verify the specificity of ABF in staining

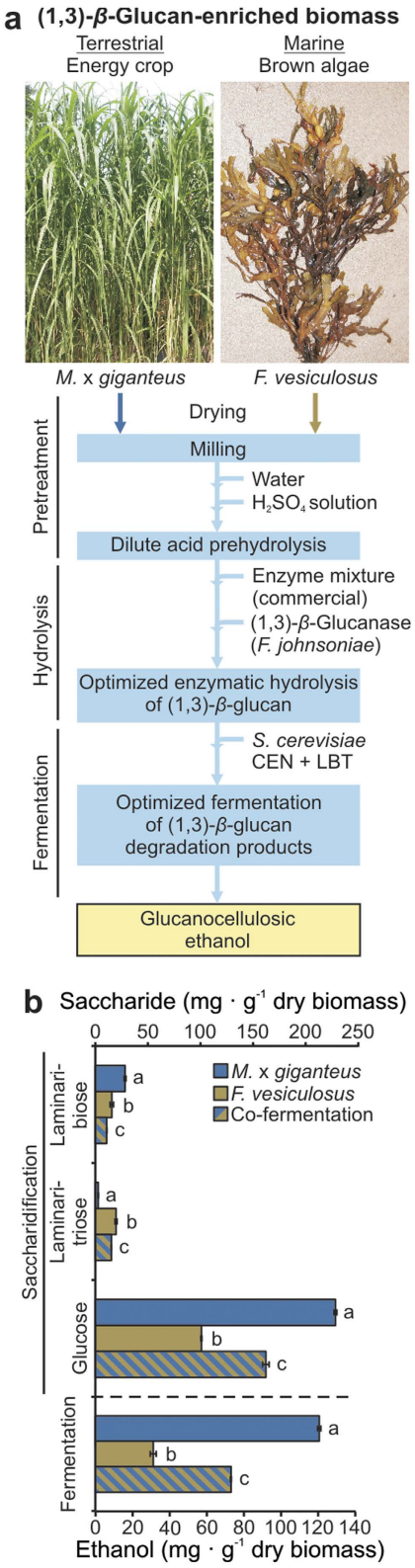

Figure 4. Co-fermentation of (1, 3)-β-glucan-enriched terrestrial and marine biomass. (**a**) Schematic overview of parallel biomass processing. Photos courtesy of Christian A. Voigt. (**b**) Saccharification efficiency and ethanol production under optimized co-processing of Miscanthus and bladderwrack biomass. Values represent the mean of two independent biological experiments. Letters a, b, c: groups with significant difference, $P < 0.05$ based on Tukey's test. Error bars represent ± SE.

(1, 3)-β-glucan. Fluorescence measurement was performed in 96-well plates with the microplate reader Synergy HT (BioTek, USA; absorbance filter: 380/20 nm, emission filter: 460/40 nm).

(1, 3;1, 4)-β-Glucan determination. Mixed linkage (1, 3;1, 4)-β-glucan in plant biomass was determined according to the manufacturer's description of the mixed-linkage beta-glucan kit (Megazyme). An additional 5 ml H_2O was added to the samples (750 mg milled leaf biomass) in the initial incubation step in a water bath (100°C). Calculation of the (1, 3;1, 4)-β-glucan content followed the instructions of the manufacturer's manual.

Confocal laser-scanning microscopy. The confocal laser-scanning microscope Zeiss LSM 780 (Carl Zeiss MicroImaging GmbH, Germany) was used for the localization of pontamine fast scarlet 4B (S4B, Sigma-Aldrich)-stained (1, 4)-β-glucan in leaf samples and ABF-stained (1, 3)-β-glucan in leaf and bladderwrack samples. To verify the specificity of ABF in staining (1, 3)-β-glucan, (1, 3)-β-glucan from *E. gracilis* (Sigma-Aldrich) as well as (1, 3;1, 4)-β-glucan from oat and barley (Megazyme) was suspended in H_2O and stained with ABF and used in CLSM. In addition, the green fluorescence protein (GFP)-tagged (1, 3)-β-glucan synthase PMR4 and single GFP in leaves of transformed Miscanthus lines was localized by CLSM. For cross sections of leaves, samples were embedded in 9% Agarose, and sections were made with a vibratome (Carl Zeiss MicroImaging). The setup for CLSM analysis of stained cell wall polymers and GFP followed the description in Ellinger *et al.*[16] and Eggert *et al.*[12].

Super-resolution microscopy. A custom modified Nikon stochastic optical reconstruction microscope (N-STORM, Nikon GmbH, Germany) was used to analyze the (1, 3)-β-glucan/(1, 4)-β-glucan polymer network of ABF and S4B stained maize and Miscanthus cross sections. The microscopic setup and image reconstruction was done according to Eggert *et al.*[12].

Treatment and fermentation of plant biomass. For pretreatment, 5 g of milled leaf biomass was mixed with 43 ml sulfuric acid (1.75% (v/v)) and autoclaved for 15 min at 120 °C. Subsequent procedures of enzymatic hydrolysis and fermentation followed the description in Meineke *et al.*[25]. To test the impact of the (1, 3)-β-glucanase from *F. johnsoniae*, 500 ng of the purified enzyme were additionally added to fermentation reactors and incubated for 24 h and 200 rpm at 37 °C. Fermentations were initiated with the inoculation of 2 ml of overnight yeast cultures of the non-adapted, laboratory strain MaV203 (MaV, Life Technologies), CEN, or CEN+LBT (generated in this study). Amounts of glucose, laminaribiose, laminaritriose, and ethanol in fermentation supernatants were quantified with a refractive index detector on an ICS-5000 system (Dionex, USA) with a HPX 87H column (Bio-Rad, USA, mobile phase 0.005 M H_2SO_4, flow rate 0.6 ml·min^{-1}, column temperature: 50 °C, refractive index detector) as described in Meineke *et al.*[25]. In addition to laminaribiose and laminaritriose, the trisaccharides glucotriose (I) (β-D-Glc-(1 → 3)-β-D-Glc -(1 → 4)-D-Glc), glucotriose (II) (β-D-Glc-(1 → 4)-β-D-Glc-(1 → 3)-D-Glc) were used as standards (all standard oligosaccharides from Megazyme) to distinguish between possible degradation products from (1, 3)-β-glucan and (1, 3;1, 4)-β-glucan.

Cloning and Miscanthus transformation. We generated two vector constructs for the transformation of Miscanthus: i) overexpression of the callose synthase gene *PMR4* from Arabidopsis (At4g03550) fused to *GFP* and ii) overexpression of single *GFP*, both under control of the 35S promoter. *PMR4-GFP* and *GFP* were amplified from the vector pCAMBIA-35S:PMR4-GFP[16] using primers in PCR reactions that provide DNA recombination sequences (*attB* sites) at their 5′ and 3′ ends (PMR4-5′attB: 5′-GGGGACAAGTTTGTACAAAAAAGCAGGCTATGAGCCTCCGCCACCGC, GFP-5′attB: 5′-GGGGACAAGTTTGTACAAAAAAGCAGGCTTGGAGATC CAAACAATGAGTAAAG, GFP-3′attB: 5′-GGGGACCACTTTGTACAAGAAAGCTGGG TTAAGCTTGAATTCTTATT TGTATA) for utilization with the Gateway cloning technology. *PMR4-GFP* and *GFP* were introduced into the plant expression vector pIPKb004[28], which provided 35S promoter-driven gene expression. Generated vector constructs containing *35S:PMR4-GFP* and *35S:GFP* expression cassettes were transformed into Agrobacterium (*Agrobacterium tumefaciens*, strain GV3101). The generation of transgenic Miscanthus lines followed the principal procedure of Agrobacterium-mediated callus transformation and selection on hygromycin-containing plant cell culture medium. Resistance to hygromycin was provided by the used plant expression vector pIBKb004. A detailed description of the transformation procedure is provided in the Supplementary Information.

Statistical analysis. Descriptive statistics including the mean and the standard error of the mean (SE) along with the Tukey range test for multiple comparison procedures in conjunction with an ANOVA were used to determine significant differences. $P < 0.05$ was considered significant.

References

1. Ash, C. *et al.* Natural systems in changing climates. Once and future climate change. Introduction. *Science* **341,** 472–473 (2013).
2. Finer, M., Jenkins, C. N., Pimm, S. L., Keane, B. & Ross, C. Oil and gas projects in the Western Amazon: threats to wilderness, biodiversity, and indigenous peoples. *Plos One* **3,** e2932, doi: 10.1371/journal.pone.0002932 (2008).

3. Sims, R. E., Mabee, W., Saddler, J. N. & Taylor, M. An overview of second generation biofuel technologies. *Bioresour. Technol.* **101,** 1570–1580 (2010).
4. Yoshida, M. *et al.* Effects of cellulose crystallinity, hemicellulose, and lignin on the enzymatic hydrolysis of *Miscanthus sinensis* to monosaccharides. *Biosci. Biotechnol. Biochem.* **72,** 805–810 (2008).
5. Hall, M., Bansal, P., Lee, J. H., Realff, M. J. & Bommarius, A. S. Cellulose crystallinity--a key predictor of the enzymatic hydrolysis rate. *FEBS J.* **277,** 1571–1582 (2010).
6. Updegraff, D. M. Semimicro determination of cellulose in biological materials. *Analyt. Biochem.* **32,** 420–424 (1969).
7. Bacic, A., Fincher, G. B. & Stone, B. A. *Chemistry, Biochemistry, and Biology of (1->3)-β-Glucans and Related Polysaccharides*. (Academic Press, 2009).
8. Burton, R. A. & Fincher, G. B. (1, 3;1, 4)-β-D-glucans in cell walls of the poaceae, lower plants, and fungi: a tale of two linkages. *Mol. Plant* **2,** 873–882 (2009).
9. Buckeridge, M., Rayon, C., Urbanowicz, B., Tine, M. & Carpita, N. Mixed linkage (1→3)(1→4)-β-D-glucans of grasses *Cereal Chem.* **81,** 115–127 (2004).
10. Scheller, H. V. & Ulvskov, P. Hemicelluloses. *Ann. Rev. Plant Biol.* **61,** 263–289 (2010).
11. Heaton, E., Dohleman, F. & Long, S. Meeting US biofuel goals with less land: the potential of Miscanthus. *Glob. Change Biol.* **14,** 2000–2014 (2008).
12. Eggert, D., Naumann, M., Reimer, R. & Voigt, C. A. Nanoscale glucan polymer network causes pathogen resistance. *Sci. Rep.* **4,** 4159, doi: 10.1038/srep04159 (2014).
13. Wilde, C. *et al.* Expression of a library of fungal beta-glucosidases in *Saccharomyces cerevisiae* for the development of a biomass fermenting strain. *Appl. Microbiol. Biotechnol.* **95,** 647–659 (2012).
14. Nataf, Y. *et al.* Cellodextrin and laminaribiose ABC transporters in *Clostridium thermocellum*. *J. Bacteriol.* **191,** 203–209 (2009).
15. Schuster, A. & Schmoll, M. Biology and biotechnology of Trichoderma. *Appl. Microbiol. Biotechnol.* **87,** 787–799 (2010).
16. Ellinger, D. *et al.* Elevated early callose deposition results in complete penetration resistance to powdery mildew in Arabidopsis. *Plant Physiol.* **161,** 1433–1444 (2013).
17. Mabeau, S. & Kloareg, B. Isolation and analysis of the cell walls of brown algae: *Fucus spiralis, F. ceranoides, F. vesiculosus, F. serratus, Bifurcaria bifurcata* and *Laminaria digitata*. *J. Exp. Bot.* **38,** 1573–1580 (1987).
18. Roesijadi, G., Jones, S. B., Snowden-Swan, L. J. & Zhu, Y. Macroalgae as a Biomass Feedstock: A Preliminary Analysis. Report No. prepared for the U.S. Department of Energy under contract DE-AC05-76RL01830, (Pacific Northwest National Laboratory, 2010).
19. Buck, B. H. & Buchholz, C. The Offshore-Ring: A new system design for the open ocean aquaculture of macroalgae. *J. Appl. Phycol.* **16,** 355–368 (2004).
20. Schorling, M., Enders, C. & Voigt, C. A. Assessing the cultivation potential of the energy crop *Miscanthus* × *giganteus* for Germany. *GCB Bioenergy*, doi: 10.1111/gcbb.12170 (2014).
21. Schiermeier, Q. Renewable power: Germany's energy gamble. *Nature* **496,** 156–158 (2013).
22. Vogel, J. P. *et al.* EST sequencing and phylogenetic analysis of the model grass Brachypodium distachyon. *Theoret. Appl. Genet.* **113,** 186–195 (2006).
23. Sigburbjorsson, B. & Micke, A. Progress in mutation breeding. In: Induced Mutation in Plants. Proceedings of an International Symposium on *Nature, Induction and Utilization of Mutation in Plants*, Vienna, 673–697. Interantional Atomic Energy Agency (1969).
24. Green, C. E. & Philips, R. L. Plant regeneration from tissue cultures of maize. *Crop Sci.* **15,** 417–421 (1975).
25. Meineke, T., Manisseri, C. & Voigt, C. A. Phylogeny in defining model plants for lignocellulosic ethanol production: A comparative study of *Brachypodium distachyon*, wheat, maize, and *Miscanthus* x *giganteus* leaf and stem biomass. *Plos One* **9,** e103580, doi: 10.1371/journal.pone.0103580 (2014).
26. Stein, M. *et al.* Arabidopsis PEN3/PDR8, an ATP binding cassette transporter, contributes to nonhost resistance to inappropriate pathogens that enter by direct penetration. *Plant Cell* **18,** 731–746 (2006).
27. Voigt, C. A., Schäfer, W. & Salomon, S. A comprehensive view on organ-specific callose synthesis in wheat (*Triticum aestivum* L.): glucan synthase-like gene expression, callose synthase activity, callose quantification and deposition. *Plant Physiol Biochem* **44,** 242–247 (2006).
28. Himmelbach, A. *et al.* A set of modular binary vectors for transformation of cereals. *Plant Physiol.* **145,** 1192–1200 (2007).

Acknowledgments

We thank E. Boles from the Goethe University Frankfurt for providing the yeast strain CEN.PK113-13D. This work was supported by a BMBF grant to C.A.V awarded to the Biocenter Klein Flottbek, University of Hamburg (FKZ0315521A).

Author Contributions

C.A.V. conceived the project rationale and wrote the manuscript. C.F. performed pretreatment, hydrolysis, and fermentation of plant and marine biomass as well as yeast strain analyses together with C.Z. C.Z. performed glucanase screening and enzyme purification. A.B. generated transgenic Miscanthus lines together with K.W. D.El. performed HPLC analyses. D.Eg. performed super-resolution localization microscopy together with R.R. M.N. performed confocal laser-scanning microscopy together with C.A.V. and C.F.

Additional Information

Supplementary information accompanies this paper at http://www.nature.com/srep

Competing financial interests: The authors declare no competing financial interests.

How to cite this article: Falter, C. *et al.* Glucanocellulosic ethanol: the undiscovered biofuel potential in energy crops and marine biomass. *Sci. Rep.* **5**, 13722; doi: 10.1038/srep13722 (2015).

SUPPLEMENTARY INFORMATION

Glucanocellulosic ethanol: the undiscovered biofuel potential in energy crops and marine biomass

Authors: Christian Falter[1]*, Claudia Zwikowics[1]*, Dennis Eggert[2,3], Antje Blümke[1], Marcel Naumann[1], Kerstin Wolff[1], Dorothea Ellinger[1], Rudolph Reimer[2], Christian A. Voigt[1]†

Affiliations:

[1]Phytopathology and Biochemistry, Biocenter Klein Flottbek, University of Hamburg, Hamburg, Germany.

[2]Heinrich Pette Institute, Leibniz Institute for Experimental Virology, Hamburg, Germany.

[3]Max Planck Institute for the Structure and Dynamics of Matter, Hamburg, Germany.

*These authors contributed equally to this work.

†Correspondence to: E-mail: christian.voigt@uni-hamburg.de (C.A.V.)

Content:

SUPPLEMENTARY INFORMATION

Supplementary Figures

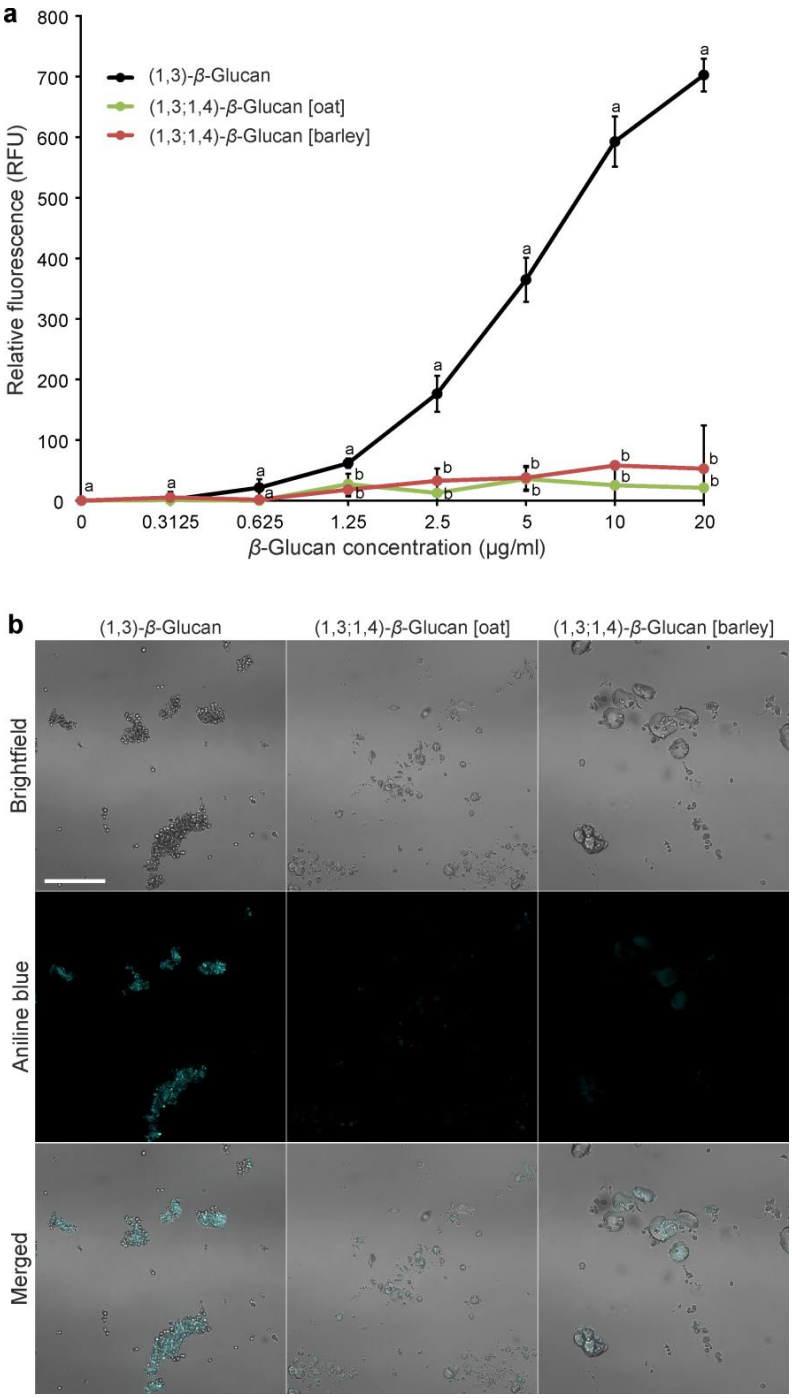

Supplementary Figure 1. Specificity of aniline blue in (1,3)-*β*-glucan determination and microscopic localization.

(1,3)-*β*-glucan from *E. gracilis* and (1,3;1,4)-*β*-glucan from oat and barley were used as reference polymers and stained with aniline blue fluorochrome (ABF). (**a**) Concentration-dependent ABF-emission of ABF-stained *β*-glucan polymers in fluorescence assays. Values represent the mean of two independent biological experiments. Letters a, b: groups with significant difference, $P < 0.05$ based on Tukey's test. Error bars represent ± SE. (**b**) Micrographs of ABF-stained *β*-glucan polymers suspended in water by confocal laser-scanning microscopy. Scale bar = 50 µm.

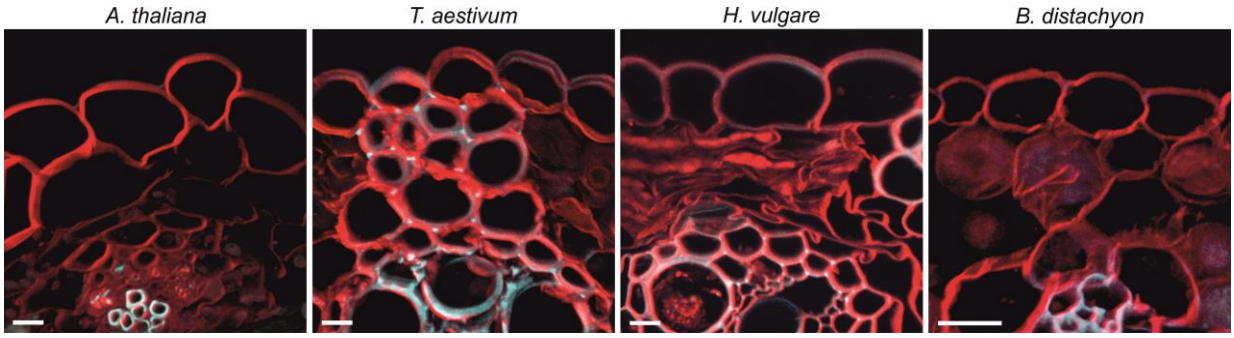

Supplementary Figure 2. Cell wall architecture of leaf cells.

Confocal laser-scanning microscopy of aniline blue fluorochrome-stained (1,3)-*β*-glucan (blue channel) and pontamine fast scarlet 4B -stained (1,4)-*β*-glucan (red channel) cross sections of leaves from the model plant Arabidopsis (*A. thaliana*), wheat (*T. aestivum*), barley (*H. vulgare*), and the model grass Brachyipodium (*B. distachyon*). Scale bars, 10 µm.

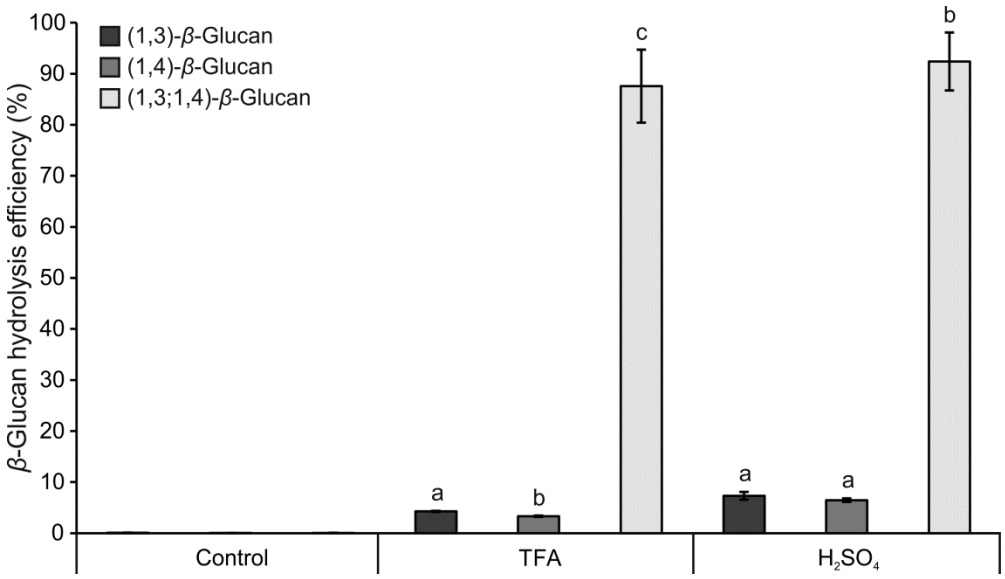

Supplementary Figure 3. Chemical hydrolysis of *β*-glucans.

β-Glucan polymers were treated with 1 M trifluoroacetic acid (TFA) and 1 M sulfuric acid (H_2SO_4) for 3 h at 105°C. Samples without TFA or H_2SO_4 treatment served as control. Amount of released glucose was used for calculation of *β*-glucan hydrolysis efficiency. Values represent the mean of two independent biological experiments. Letters a, b, c: groups with significant difference, $P < 0.05$ based on Tukey's test. Error bars represent ± SE.

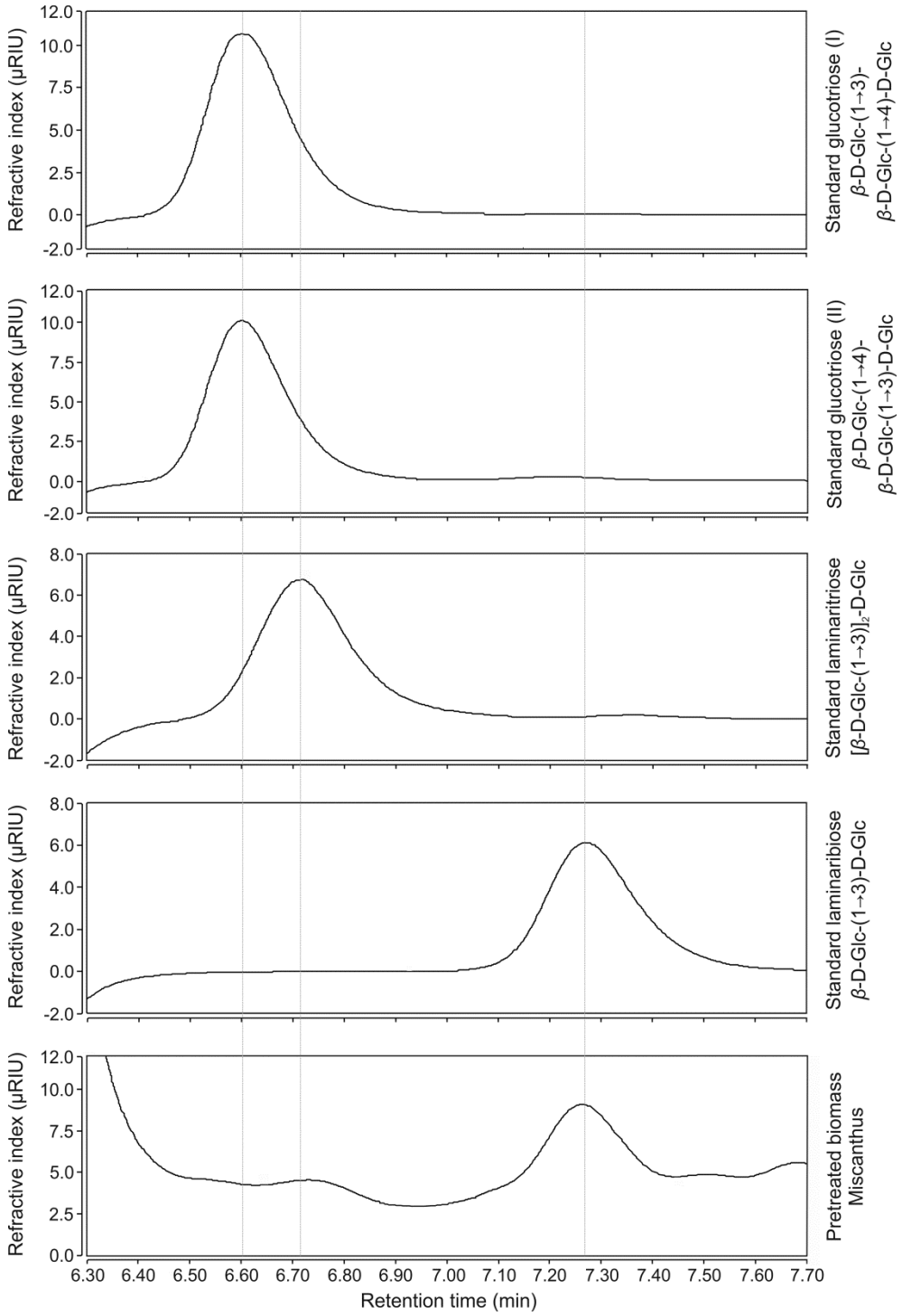

Supplementary Figure 4. Chromatograms of *β*-glucan di- and trimers using an RI detector.

Chromatograms of standard *β*-glucan di-and trimers (concentration: 0.4 µg·ml^{-2}) were obtained with an HPLC-coupled refractive index (RI) detector. Chromatogram of thermo-chemically and enzymatically pretreated Miscanthus biomass as an example for laminaribiose and –triose detection in biomass samples. Grey, dotted lines indicate retention times of (1,3;1,4)-*β*-glucan trimers (left), laminaritriose (middle), and laminaribiose (right). Two independent biological experiments gave similar results.

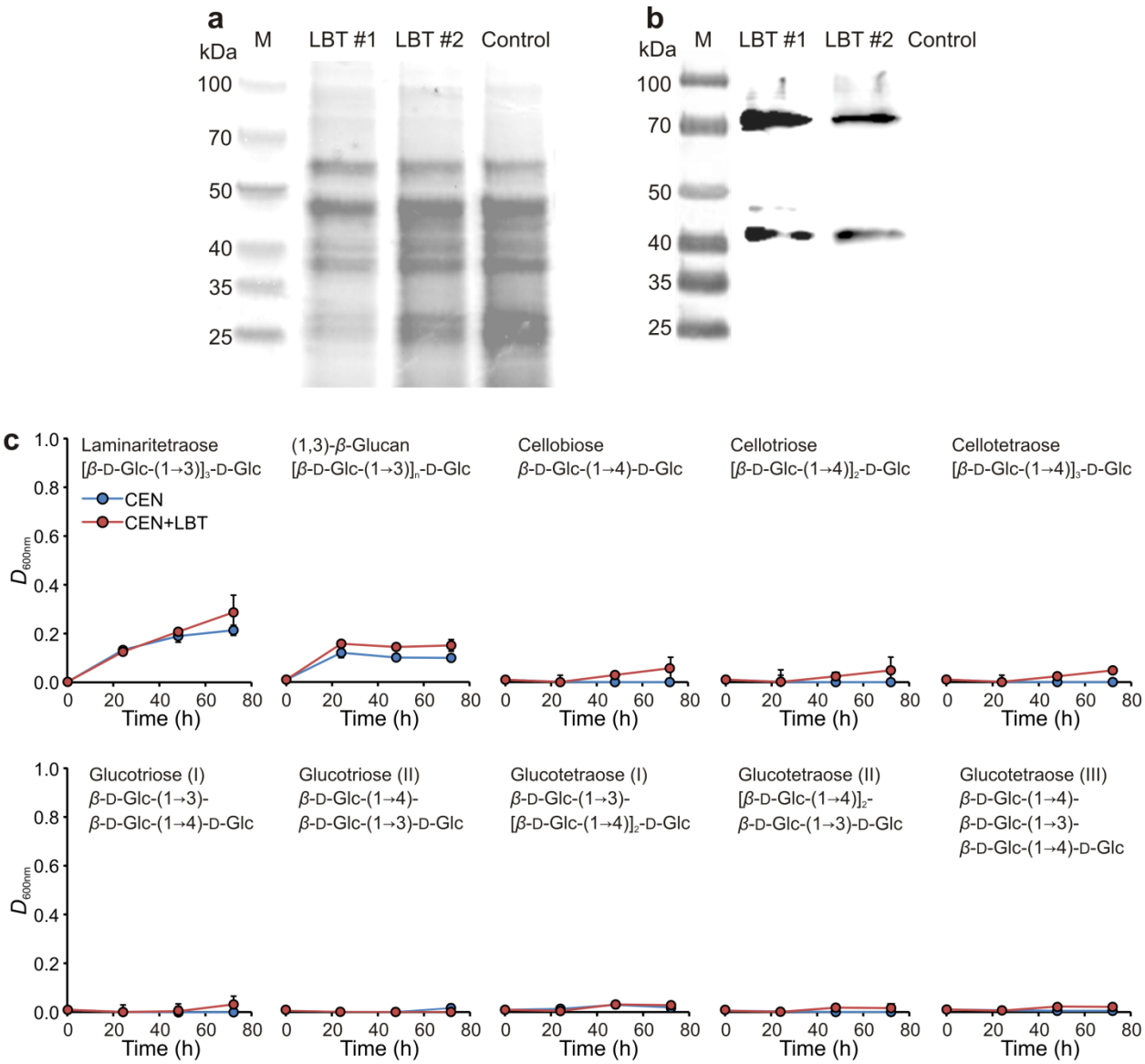

Supplementary Figure 5. Characterization of laminaribiose transporter-expressing yeast strains. Yeast strain CEN was transformed with yeast expression vector carrying bacterial laminaribiose ABC transporter (LBT) from *C. thermocellum*. Two independent clones (CEN+LBT #1 and #2) were randomly chosen for characterization. (**a**) Separation of total protein extracts on SDS-PAGE as loading control prior Western blot analysis. Proteins stained with Coomassie. Protein samples derived from of CEN+LBT strains #1 and #2 and control strain carrying the empty vector. M, Spectra Multicolor Broad Range Ladder (Thermo Scientific). (**b**) Western blot analysis of protein samples as indicated in (a) using a primary anti-His antibody. Expected size of LBT (incl. C-terminal His tag): 42 kDa. Additional hybridization of LBT-His at approx. 80 kDa indicated possible dimerization. (**c**) In vitro growth assays of the CEN and the CEN+LBT (strain #2) yeast strains on substrates as indicated. Values represent the mean of two independent biological experiments. No significant difference, $P < 0.05$ based on Tukey's test. Error bars represent ± SE.

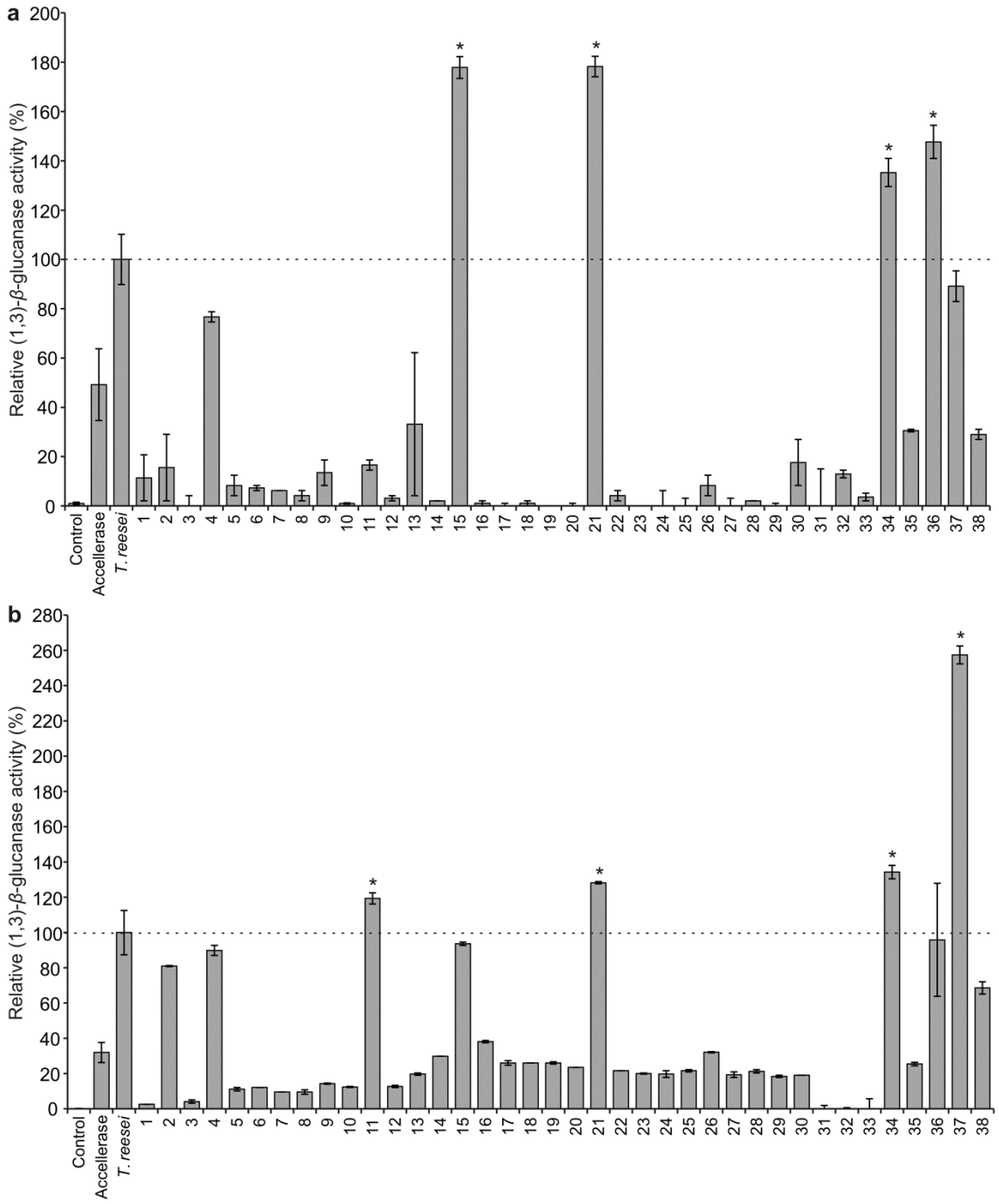

Supplementary Figure 6. (1,3)-*β*-Glucanase screening.

(1,3)-*β*-Glucanases (see supplementary table 1 for the sources of each of the numbered enzymes) were heterologously expressed und purified from *E. coli* via N-terminal His-tag fusion. Enzymatic activity of commercially available (1,3)-*β*-glucanase from *T. reesei* (Sigma-Aldrich) served as reference, Accellerase 1500 cellulose enzyme complex (Danisco) as additional hydrolysis control. (1,3)-*β*-glucan from *E. gracilis* (**a**) or *L. digitata* (**b**) were used as substrate in activity assays (conditions: pH 6, 37°C). (to be continued on next page)

Supplementary Figure 6. (1,3)-*β*-Glucanase screening. (continued)

Amount of released glucose was used for calculation of (1,3)-*β*-glucanase activity. Values represent the mean of two independent biological experiments. *Enzymatic activity significantly higher than reference activity from *T. reesei* (1,3)-*β*-glucanase at $P < 0.05$ based on Tukey's test. Error bars represent ± SE. (1,3)-*β*-glucanases #11, #15#, #21, #34, #36, and #37 were selected for further characterization due to highest enzymatic activity

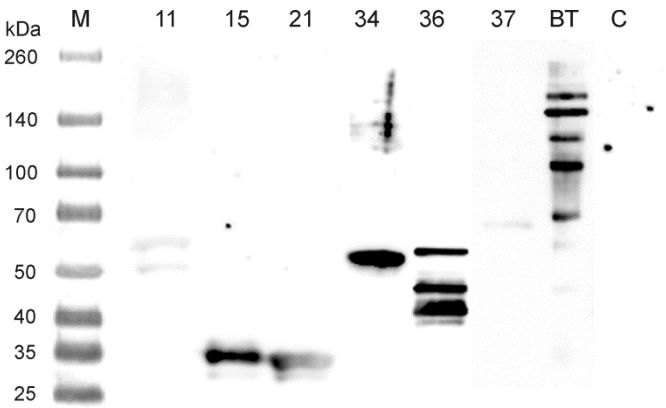

Supplementary Figure 7. Verification of (1,3)-*β*-glucanase purification and protein size.

Western blot analysis of purified (1,3)-*β*-glucanases showing higher enzymatic activity than the reference enzyme from *T. reesei* in (1,3)-*β*-glucanase screening (Supplementary Fig. 4) using an anti-His antibody. Protein extraction and purification from empty vector *E. coli* strain served as control (C). Expected protein sizes of tested (1,3)-*β*-glucanases (#11 - #37) can be found in supplementary table 1. M, Spectra Multicolor Broad Range Ladder (Thermo Scientific); BT, Biotinylated Protein Ladder (Cell Signaling Technology, USA).

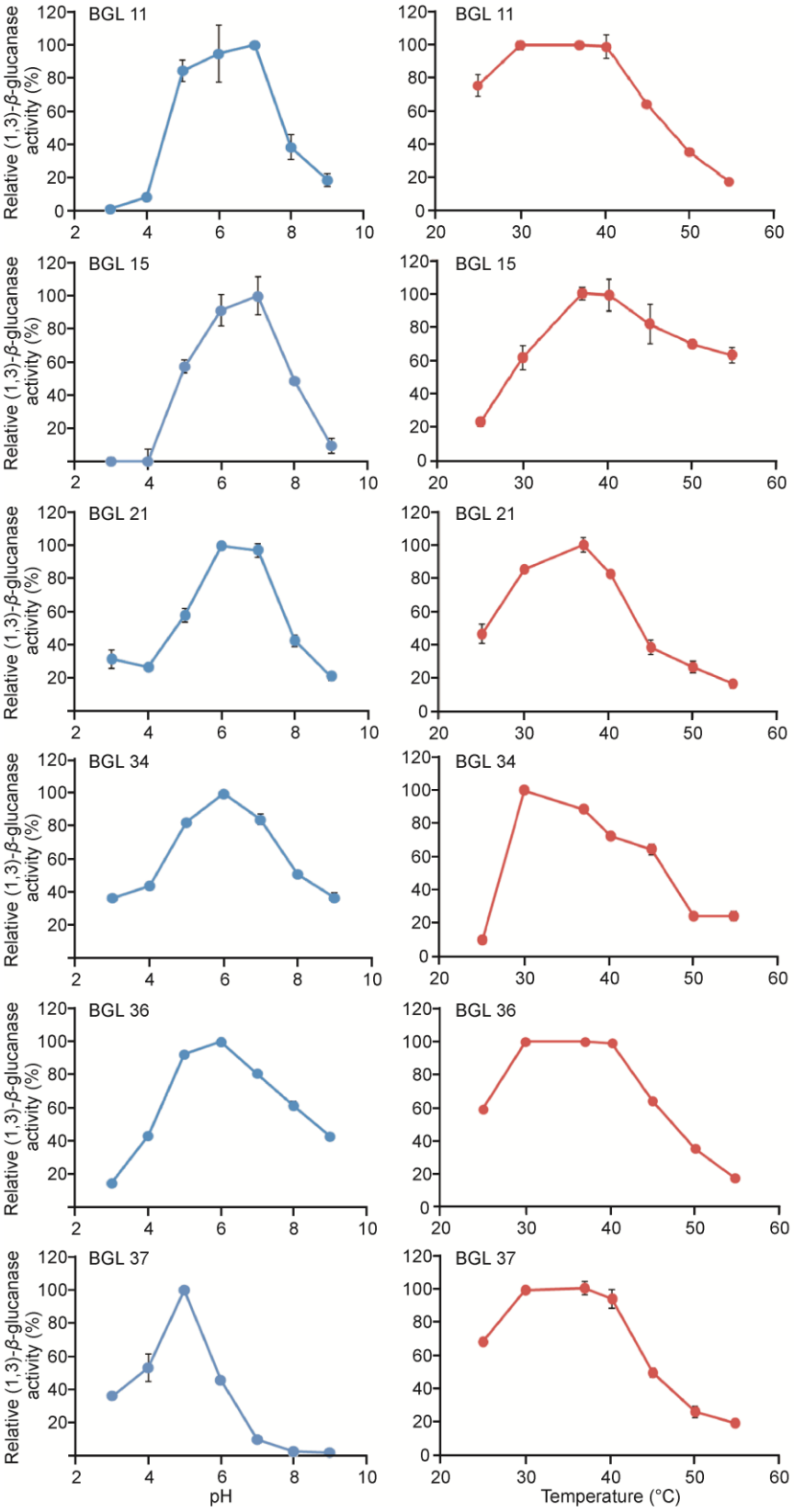

Supplementary Figure 8.

Characterization of enzymatic activity of (1,3)-*β*-glucanases.
Determination of optimal pH and temperature range of purified (1,3)-*β*-glucanases (BGL #11 – BGL #37, Supplementary Tab. 1). (1,3)-*β*-glucan from *E. gracilis* was used as substrate in activity assays under conditions as indicated. Amount of released glucose was used for calculation of (1,3)-*β*-glucanase activity. Values represent the mean of two independent biological experiments. Error bars represent ± SE.

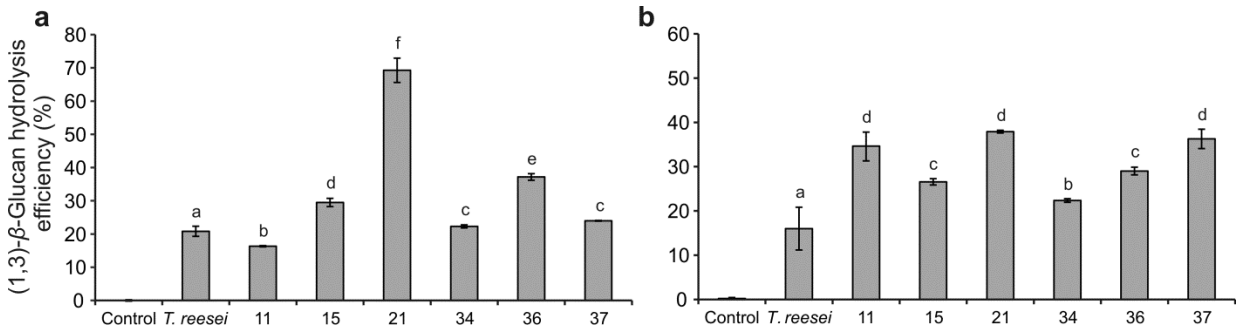

Supplementary Figure. 9. Enzymatic activity of (1,3)-*β*-glucanases under optimal conditions.

Determination of enzymatic activity of purified (1,3)-*β*-glucanases (#11 - #37, Supplementary Tab. 1) under optimal enzymatic activity conditions (Supplementary Fig. 6) for each protein. Enzymatic activity of commercially available (1,3)-*β*-glucanase from *T. reesei* (Sigma-Aldrich) served as reference. (1,3)-*β*-glucan from *E. gracilis* (**a**) or *L. digitata* (**b**) was used as substrate in activity assays. Amount of released glucose was used for calculation of (1,3)-*β*-glucan hydrolysis efficiency of each enzyme. Values represent the mean of three independent biological experiments. Letters a, b, c, d, e, f: groups with significant difference, $P < 0.05$ based on Tukey's test. Error bars represent ± SE.

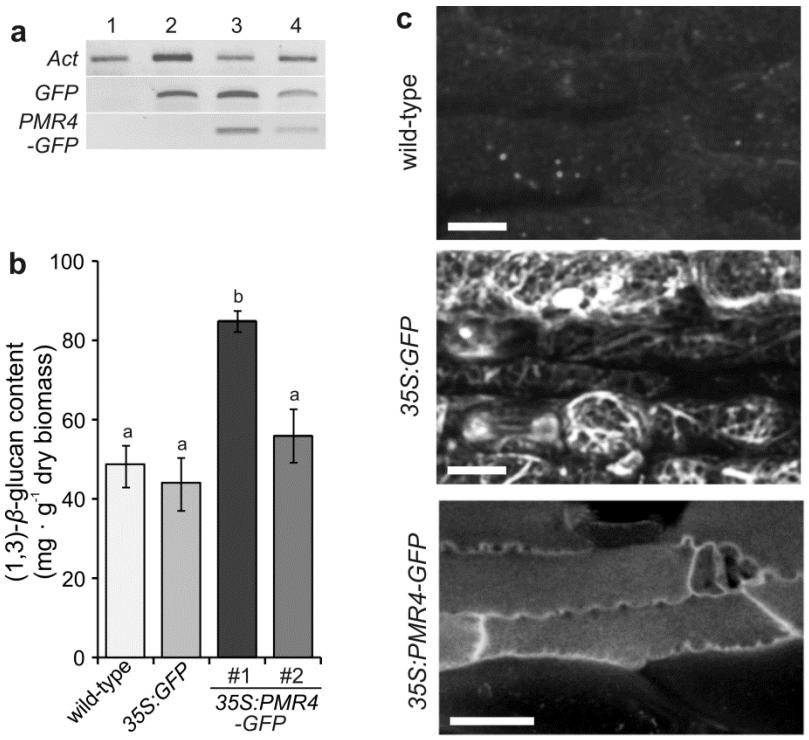

Supplementary Figure 10. Characterization of transgenic Miscanthus lines.

Agrobacterium-mediated transformation of Miscanthus (*M.* x *giganteus*) calli was used to generate transgenic Miscanthus lines. For increasing (1,3)-*β*-glucan content, the transgenic Miscanthus lines *35S:PMR4-GFP* #1 and #2 with an overexpression of the (1,3)-*β*-glucan synthase gene *PMR4* (*POWDERY MILDEW RESISTANT 4*) from Arabidopsis fused to the green fluorescence protein GFP were generated. A *GFP* overexpression line (*35S:GFP*) served as control. (**a**) *GFP* and *PMR-GFP* gene expression in leaf tissue of transgenic Miscanthus lines. Gene expression in non-transgenic wild-type plants was used as control. RNA was isolated from leaf tissue and used as template in complementary DNA generation. *Actin* (*Act*) gene expression served as reference. A repeat experiment gave similar results. Miscanthus lines: 1, wild-type; 2, *35S:GFP*; 3, *35S:PMR4-GFP* #1, 4, *35S:PMR4-GFP* #2. (**b**) Determination of (1,3)-*β*-glucan content in leaf tissue of Miscanthus wild-type and transgenic lines. Values represent the mean of three independent biological experiments. Letters a, b: groups with significant difference, $P < 0.05$ based on Tukey's test. Error bars represent ± SE. Based on the results of the (1,3)-*β*-glucan content, transgenic Miscanthus line *35S:PMR4-GFP* #1 was used in all subsequent experiments and referred to as "*35S:PMR4-GFP*". (**c**) Confocal laser-scanning microscopy to localize the fusion protein PMR4-GFP in the Miscanthus overexpression line *35S:PMR4-GFP* and single GFP in the control line *35S:GFP*. Micrographs display the 3D projection of epidermal leaf cells; shown is the view from the outside to the leaf surface. Micrographs are representative for the localization of single GFP in cytosolic strands in line *35S:GFP* and of PMR4-GFP at the plasma membrane in line *35S:PMR4-GFP* after examining at least 25 regions on 5 independent leaves from each line. Scale bars, 20 µm.

Supplementary Tables

Supplementary Table 1.

Origin of (1,3)-β-glucanase genes used for heterologous expression in *E. coli*. Enzyme size calculated on the basis of the amino acid sequence encoded by the respective (1,3)-β-glucanase gene.

No.	Species	Kingdom	Enzyme size [kDa]	GenBank
1	*Acremonium cellulolyticus* (*Talaromyces cellulolyticus*)	Fungi	95.8	BD168028.1
2	*Agaricus bisporus*	Fungi	50.7	XM_006454084.1
3	*Agaricus bisporus*	Fungi	19.5	X92961.1
4	*Aspergillus flavus*	Fungi	101.4	XM_002374364.1
5	*Aspergillus flavus*	Fungi	50.9	XM_002376609.1
6	*Aspergillus fumigatus* (strain Af293)	Fungi	43.6	XM_741253.2
7	*Aspergillus fumigatus* (strain Af293)	Fungi	86.5	XM_741429.1
8	*Aspergillus fumigatus* (strain Af293)	Fungi	111.1	XM_745080.1
9	*Aspergillus fumigatus* (strain Af293)	Fungi	94.1	XM_745984.1
10	*Aspergillus fumigatus* (strain Af293)	Fungi	100.9	XM_745719.1
11	*Aspergillus fumigatus* (strain Af293)	Fungi	49.5	XM_745017.1
12	*Aspergillus fumigatus* (strain Af293)	Fungi	95.8	XM_742417.1
13	*Aspergillus fumigatus* (strain Af293)	Fungi	90.6	XM_749766.1
14	*Bacillus circulans*	Bacteria	136.9	DI025015.1
15	*Bacillus clausii* (strain KSM-K16)	Bacteria	35.4	NC_006582.1
16	*Candida albicans* (strain SC5314)	Fungi	128.7	XM_716200.1
17	*Chaetomium thermophilum*	Fungi	70.3	DQ888228.1
18	*Chaetomium thermophilum*	Fungi	99.4	EF648280.1
19	*Clostridium thermocellum*	Bacteria	100.8	L04735.1
20	*Coccidioides immitis* (strain RS)	Bacteria	57.4	XM_001245402.1
21	*Flavobacterium johnsoniae* (strain UW101)	Bacteria	33.8	NC_009441.1
22	*Hypocrea lixii* (*Trichoderma harzianum*)	Fungi	85.9	CAA58889.1
23	*Hypocrea lixii* (*Trichoderma harzianum*)	Fungi	56.4	ACM42429.1
24	*Hypocrea lixii* (*Trichoderma harzianum*)	Fungi	52.5	FJ589724.1
25	*Lycopersicon esculentum* (tomato)	Plantae	41.0	X74906.1
26	*Lycopersicon esculentum* (tomato)	Plantae	41.0	X74905.1
27	*Neosartorya fischeri* (strain NRRL 181)	Fungi	38.3	NW_001509760.1
28	*Neurospora crassa* (strain OR74A)	Fungi	109.6	XM_952460.1
29	*Oryza sativa* (rice)	Plantae	25.5	NM_001066906.1
30	*Oryza sativa* (rice)	Plantae	56.1	NM_001057345.1

SupplementaryTable 1. (continued)

No.	Species	Kingdom	Enzyme size [kDa]	GenBank
31	*Oryza sativa* (rice)	Plantae	45.9	NM_001070740.1
32	*Stachybotrys echinata*	Fungi	31.4	AF435067.1
33	*Streptomyces avermitilis* (strain MA-4680)	Bacteria	51.1	BA000030.3
34	*Streptomyces avermitilis* (strain MA-4680)	Bacteria	47.0	NC_003155.4
35	*Streptomyces sioyaensis*	Bacteria	51.4	AF217415.1
36	*Streptomyces sp.* (strain AP77)	Bacteria	43.6	AB127079.1
37	*Trichoderma asperellum*	Fungi	107.9	EU314718.1
38	*Trichoderma viride*	Fungi	85.3	EF176582.1

Supplementary Table 2.

DNA sequence of gene encoding the laminaribiose ABC transporter from *C. thermocellum* after codon usage optimization for yeast (GeneArt GeneOptimizer, Life Technologies).

ATGAAGAAGTTCTTGGCCTTGTTGTTGTCCGTTATCATCGTTTTTTCTTTGACTGCTTG
TGGTGGTAAGAACTCTGGTAACAATTCTAACAACTCCTCCAACAACAACTCCAGTAA
CAATACTGGTGGTAAAAAGATCAAGATCGGTATGGTTACTGATGTTGGTGGTGTTAA
TGACGGTTCCTTTAATCAATCTGCTTGGGAAGGTTTACAAAGAGCCCAAAAAGAATT
GGGTGTTGAAGTTAGATATGCTGAATCTGCTACTGATGCTGATTACGCTCCAAATATT
GAAGCCTTCATTGATGAAGGTTACGACTTGATTATTTGCGTCGGTTATATGTTGGCTG
ATGCTACTAGAAAAGCTGCTGAAGCTAATCCAAATCAAAAGTTCGCCATTATCGATG
ATGCCTCCATTGATTTGCCAAACGTTACTTGTTTGATGTTTGAACAATCCCAAGCCTC
TTACTTGGTTGGTTTGGTTGCTGGTAAAATGACTAAGACTAACAAGGTTGGTTTCGTC
GTTGGTATGGTTTCTCAAACTATGAACGAATTCGGTTACGGTTATTTGGCTGGTGTCA
AAGATGCTAATCCTAACGCTACCATCTTGCAATTCAATGCCAACTCTTTCTCTTCTAC
TGAAACTGGTAAATCTGCTGCTACTACCATGATTACTAATGGTGCCGATGTTATTTTT
CATGCTGCTGGTGGTACTGGTTTGGGTGTTATTGAAGGTTGTAAAGATGCAGGTAAA
TGGGCCATTGGTGTTGATTCTGATCAATCTCCATTGGCCCCAGAAAACATTTTGACAT
CTGCAATGAAGAGAGTTGATAACGCCTGTTTCGATATTGCTAAGGCTGTAAAAGAAG
GTAACGTTAAGCCAGGTATTATCACCTACGATTTGAAATCTGCCGGTGTTGATATTGC
TCCAACTACTACTAATTTGCCTAAAGAAGTTTTGGACTACGTCAATCAAGCCAAGCA
AGATATTATCAACGGTAAGATCACTGTCCCAAAGACTAAGGCTGAATTTGAAGCTAA
GTACGGTAACATCTACGAATTGGATGACG

Supplementary Video Legends

Supplementary Video 1. Direct interaction of (1,3)-*β*-glucan and (1,4)-*β*-glucan macrofibrils determines cell wall architecture of epidermal leaf cells in maize.

3D Super-resolution imaging of maize epidermal leaf cell walls co-stained with aniline blue fluorochrome for specific (1,3)-*β*-glucan detection (blue channel) and pontamine fast scarlet 4B for specific (1,4)-*β*-glucan detection (red channel) by super-resolution localization microscopy. Video generation with Bitplane Imaris 7.6.1. (Bitplane, Switzerland). Interaction of (1,3)-*β*-glucan and (1,4)-*β*-glucan cell wall polymers mainly based on direct macrofibrils interaction.

Supplementary Video 2. Direct interaction of (1,3)-*β*-glucan and (1,4)-*β*-glucan macrofibrils determines cell wall architecture of epidermal leaf cells in Miscanthus.

3D Super-resolution imaging of Miscanthus epidermal leaf cell walls co-stained with aniline blue fluorochrome for specific (1,3)-*β*-glucan detection (blue channel) and pontamine fast scarlet 4B for specific (1,4)-*β*-glucan detection (red channel) by super-resolution localization microscopy. Video generation with Bitplane Imaris 7.6.1. (Bitplane, Switzerland). Interaction of (1,3)-*β*-glucan and (1,4)-*β*-glucan cell wall polymers stronger than in maize and mainly based on direct macrofibrils interaction and additional partial surrounding of (1,4)-*β*-glucan macrofibrils by (1,3)-*β*-glucan macrofibrils.

Supplementary Video 3. (1,3)-*β*-Glucan deposition in the central pith region of bladderwrack blades.

High-resolution imaging of elongated cells within the central pith region of bladderwrack blades stained with aniline blue fluorochrome for specific (1,3)-*β*-glucan detection by confocal laser-scanning microscopy. Video generation from maximum intensity reconstruction using integral functions of the ZEN 2010 (Zeiss MicroImaging GmbH) operating software. Scattered (1,3)-*β*-glucan deposition pattern in elongated cells of the central pith region.

Supplementary Video 4. (1,3)-*β*-Glucan deposition in the cortex and epidermis of bladderwrack blades.

High-resolution imaging of cortex and epidermal cells of bladderwrack blades stained with aniline blue fluorochrome for specific (1,3)-*β*-glucan detection by confocal laser-scanning microscopy. Video generation from maximum intensity reconstruction using integral functions of the ZEN 2010 (Zeiss MicroImaging GmbH) operating software. Deposition of (1,3)-*β*-glucan in relatively compact, intracellular layer in cortex and especially epidermis cells.

Supplementary Methods

Heterologous (1,3)-*β*-glucanase expression and purification

Full length cDNAs encoding (1,3)-*β*-glucanases from different organisms (Supplementary Tab. 1) were synthesized with DNA recombination sequences (*attB* sites) at their 5' and 3' ends (GeneArt, Germany) for subsequent utilization with the Gateway cloning technology (Life Technologies, USA). After introduction into the donor vector pDONR221 (Life Technologies) via BP Clonase-mediated recombination, the (1,3)-*β*-glucanase genes were introduced into the *Escherichia coli* expression vector pDEST17 (Life Technologies), providing N-terminal fusion with 6xHis after successful expression, via LR Clonase-mediated recombination. Expression vectors were transformed into *E. coli* strain Rosetta (DE3). *E. coli* cultures were set to D_{600} = 0.5 - 0.8 in Luria-Bertani (LB) bacterial growth media (supplemented with 100 $\mu g \cdot ml^{-1}$ ampicillin and 30 $\mu g \cdot ml^{-1}$ chloramphenicol) and cultivated overnight at 25°C. Heterologous gene expression was induced by adding IPTG (0.5 mM) to the cultures, which were then cultivated overnight at 17°C and 160 rpm to reduce inclusion body formation. For (1,3)-*β*-glucanase purification, *E. coli* cultures were centrifuged and the cell pellets washed with Tris-HCl (20 mM). Cell pellets were then resuspended in native binding buffer (0.2 M NaH_2PO_4, 0.2 M Na_2HPO_4, 29.22 $mg \cdot ml^{-1}$ NaCl) supplemented with 5 $ml \cdot g^{-1}$ pellet imidazole (50 mM, pH 7.4). Lysozyme (0.2 $mg \cdot ml^{-1}$) and PMSF (1 mM) were added, and samples were incubated on ice for 1 h for cell lysis. After sonication, DNA was degraded with the addition of DNase (5 $\mu g \cdot ml^{-1}$) and $MgCl_2$ (10 mM) and an incubation on ice for 15 min. Cell lysates were centrifuged (20 min, 4000 rpm, 4°C) and supernatant containing the His-tagged (1,3)-*β*-glucanases were incubated with Ni-NTA agarose (Qiagen, Germany) in native binding buffer. Washing and elution of His-tagged (1,3)-*β*-glucanases from Ni-NTA agarose followed the manufacturer's instructions (native elution buffer with 500 mM imidazole). For subsequent activity assays, the buffer of the protein samples was exchanged (new buffer conditions: pH 6, 87.7 mM NaH_2PO_4, 12.3 mM Na_2HPO_4) by using Amicon ultra centrifugal filters (Merck Millipore, Germany).

(1,3)-*β*-glucanase activity assay

Purified (1,3)-*β*-glucanases at a final concentration of 100 $\mu g \cdot ml^{-1}$ were incubated overnight in 100 ml activity buffer (pH 6, 87.7 mM NaH_2PO_4, 12.3 mM Na_2HPO_4) containing 500 $\mu g \cdot ml^{-1}$ (1,3)-*β*-glucan from *E. gracilis* or *Laminaria digitata* (Sigma-Aldrich) as substrate at 37°C. Commercially available (1,3)-*β*-glucanase from *T. reesei* (Sigma-Aldrich) served as reference.

Release of glucose due to (1,3)-*β*-glucan hydrolysis was used to determine (1,3)-*β*-glucanase activity. Quantification of glucose followed the description from Stitt *et al.*[1] in photometrical assays in 96-well plates.

To determine the optimal temperature of (1,3)-*β*-glucanase activity, enzyme samples were incubated overnight in the activity buffer as described above, however, at temperatures ranging from 25°C to 55°C. pH dependency of (1,3)-*β*-glucanase activity was measured from overnight incubations at 37°C using an acetate buffer system in the range from pH 3 to pH 5 and a phosphate buffer system in the range from pH 6 to pH 9 [2].

Laminaribiose transporter yeast strain generation

To improve utilization of the (1,3)-*β*-glucan hydrolysis products laminaribiose and laminaritriose, the yeast (*S. cerevisiae*) strain CEN.PK113-13D (CEN, *MATα MAL2-8^c SUC2 ura3-52*) was transformed with an expression vector carrying the bacterial laminaribiose ABC transporter (LBT) from *C. thermocellum*[3]. For expression vector generation, the full length cDNA encoding LBT was codon optimized for yeast expression (sequence see Supplementary Tab. 2) and synthesized with DNA recombination sequences (*attB* sites) at their 5' and 3' ends (ShineGene, China) for subsequent utilization with the Gateway cloning technology. After introduction into the donor vector pDONR221 via BP Clonase-mediated recombination, the *LBT* gene was introduced into the yeast expression vector pYES-DEST52-GAP, providing C-terminal fusion with 6xHis after successful expression, via LR Clonase-mediated recombination. The vector pYES-DEST52-GAP was generated by replacing the inducible galactokinase (GAL1) promoter of the expression vector pYES-DEST52 (Life technologies) by the constitutive glyceraldehyde-3-phopshate dehydrogenase (GAP) promoter of the *Pichia pastoris* expression vector pGAPZ (Life technologies). The GAP promoter sequence was amplified via PCR reaction using primers that provide endonuclease recognition sites at the 5'-end (*Spe*I, GAP-5'Spe: 5'-CGAAAACACTAGTTAAGGGAT TTTGGTC) and the 3'-end (*Acc*III, GAP-3'Acc: 5'-GCTCACCGTCTTTCATTGTCCGGA) of the amplified PCR fragment. After *Spe*I/*Acc*III endonuclease treatment of the GAP fragment, it was cloned into the likewise prepared yeast expression vector pYES-DEST52 via sticky-end ligation.

The yeast strain CEN was transformed with the respective expression vector containing the *LBT* gene under the control of the constitutive GAP promoter using the lithium-acetate method for yeast transformation[4]. Based on its slightly better growth characteristics on glucose,

laminaribiose, and laminaritriose (Fig. 2b), the transformed CEN strain CEN+LBT #2 was used in all subsequent growth assays and biomass fermentations and referred to as "CEN+LBT".

Yeast growth assay

Overnight cultures (28°C, 150 rpm) of the CEN and CEN+LBT yeast strains were cultivated in 5 ml SD liquid medium (6.7 $g \cdot l^{-1}$ yeast nitrogen base w/o amino acids (BD, USA), 0.78 $g \cdot l^{-1}$ dropout powder w/o uracil (Clontech, USA), 20 $g \cdot l^{-1}$ glucose, and with (CEN) or without (CEN+LBT) 40 $mg \cdot l^{-1}$ uracil (Sigma-Aldrich), pH 5,8). Yeast cultures were centrifuged and pellets washed with H_2O. After additional centrifugation, the pellet was resuspended in 10 ml H_2O. Growth assays were performed in 96-well plates in 200 µl minimal medium (SD liquid medium without glucose) with a carbon source concentration of 1 $g \cdot l^{-1}$. Yeast starting concentrations were set to D_{600} = 0.01. Carbon sources tested were glucose, (1,3)-*β*-glucan from *E. gracilis*, laminaribiose (this and all following oligosaccharides from Megazyme), laminaritriose, laminaritetraose, cellobiose, cellotriose, cellotetraose, glucotriose (I) (*β*-D-Glc-(1→3)-*β*-D-Glc-(1→4)-D-Glc), glucotriose (II) (*β*-D-Glc-(1→4)-*β*-D-Glc-(1→3)-D-Glc), glucotetraose (I) (*β*-D-Glc-(1→3)-[*β*-D-Glc-(1→4)]$_2$-D-Glc), glucotetraose (II) ([*β*-D-Glc-(1→4)]$_2$-*β*-D-Glc-(1→3)$_2$-D-Glc), and), glucotetraose (III) (*β*-D-Glc-(1→4)-*β*-D-Glc-(1→3)$_2$-*β*-D-Glc-(1→4)-D-Glc). 96-well plates with growth assays were incubated at 28°C and 150 rpm for 72 h. D_{600} was measured every 24 h in a microplate reader (BioTek).

Western blot analysis

Expression and size of the six (1,3)-*β*-glucanases #11, #15, #21, #34, #36, and #37 (Supplementary Tab. 1), which showed highest enzymatic activity (Supplementary Figs. 3 and 6), and of LBT in the yeast strains CEN+LBT #1 and #2 were confirmed via Western blot analysis. Proteins were separated on an SDS-PAGE and transferred on nitrocellulose membranes using transfer buffer (Thermo Scientific, USA) in a Trans-Blot electrophoretic transfer cell (Biorad, USA). After protein transfer, membranes were washed and additionally treated with the Pierce Western blot signal enhancer kit (Thermo Scientific) according to the manufacturer's instructions. Blocking of membranes was done in Tris-buffered saline with Tween 20 (TBST) buffer containing 5 % skimmed milk powder. Membranes were then incubated overnight at 8°C with an anti-His antibody (Roche, Germany) as primary antibody in TBST with 1 % skimmed milk powder. A secondary, horseradish peroxidase (HRP)-conjugated anti-mouse IgG antibody

(Promega, Germany) was used according to the manufacturer's instructions. Hybridization of the antibodies with the respective proteins was detected by chemiluminescence using the SuperSignal West Pico substrate (Thermo Scientific). Identity of tested proteins was additionally verified by mass spectrometry.

Chemical hydrolysis of *β*-glucans

5 mg of (1,3)-*β*-glucan from *E. gracilis*, the (1,4)-*β*-glucan cellulose, and the mixed-linkage (1,3;1,4)-*β*-glucan from barley (all glucans from Sigma-Aldrich) were treated with 1 ml of 1 M trifluoroacetic acid or 1 M sulfuric acid for 3 h at 105°C. The amount of released glucose was quantified with a refractive index detector as described above.

Miscanthus transformation

For callus induction, young, immature inflorescences from Miscanthus were surface sterilized with sodium hypochlorite (2 %) and then with ethanol (70 %), each for 5 min. After rinsing with H_2O, inflorescences were cut into 1 cm pieces and transferred on callus induction medium (CIM) (30 $g \cdot l^{-1}$ sucrose, 4.3 $g \cdot l^{-1}$ Murashige and Skoog Basal Salt Mixture (MS), 2 $g \cdot l^{-1}$ phytagel, 112 $mg \cdot l^{-1}$ vitamin B5, $MgCl_2$ (final concentration 3.69 mM), 2,4-dichlorophenoxyacetic acid (13.57 µM), 6-benzylaminopurine (0.44 µM), L-proline (24.33 mM), pH 5.8) and incubated in the dark at 28°C for 3 – 4 weeks. For Agrobacteria-mediated callus transformation, calli were incubated with infiltration medium (IM) (10 $g \cdot l^{-1}$ sucrose, 4.3 $g \cdot l^{-1}$ MS, 10 $g \cdot l^{-1}$ mannitol, acetosyringone (final concentration 2.29 µM), pH 5.5) containing Agrobacteria strains (carrying vector constructs as described above) on CIM plates for 30 min. After incubation, Agrobacterium suspension was removed. Calli were dried on filter paper, transferred onto filter paper soaked with IM, and incubated in petri dishes at room temperature in the dark for 7 d. To remove Agrobacteria after co-incubation, calli were first rinsed with H_2O and then with a ticarcillin disodium mixture solution (500 $mg \cdot ml^{-1}$, Duchefa, Netherlands). After overnight incubation in the ticarcillin disodium mixture solution, calli were rinsed with water, dried on filter paper, and transferred on selection medium (30 $g \cdot l^{-1}$ sucrose, 4.3 $g \cdot l^{-1}$ MS, 2 $g \cdot l^{-1}$ phytagel, 112 $mg \cdot l^{-1}$ vitamin B5, 224 $mg \cdot l^{-1}$ ticarcillin disodium mixture, 50 $mg \cdot l^{-1}$ hygromycin, $MgCl_2$ (final concentration 3.69 mM), 2,4-dichlorophenoxyacetic acid (13.57 µM), 6-benzylaminopurine (0.44 µM), L-proline (173.76 µM), glycine (266.67 µM), L-asparagine monohydrate (66.6 µM), pH 5.8). After incubation in the dark at 28°C for 2 – 3 weeks, surviving calli were transferred on regeneration medium (20 $g \cdot l^{-1}$ sucrose, 4.3 $g \cdot l^{-1}$ MS, 10 $g \cdot l^{-1}$ mannitol, 2 $g \cdot l^{-1}$ phytagel, 112 $mg \cdot l^{-1}$

vitamin B5, 124.8 $mg \cdot l^{-1}$ ticarcillin disodium mixture, 1-naphthaleneacetic acid (final concentration 2.69 µM), kinetin (2.32 µM), pH 5.8) and incubated at 16 h of light at 25°C. Regenerated plants (approximate size 5 mm) were then transferred on germination medium (30 $g \cdot l^{-1}$ sucrose, 4.3 $g \cdot l^{-1}$ MS, 14 $g \cdot l^{-1}$ activated charcoal, 2 $g \cdot l^{-1}$ phytagel, 112 $mg \cdot l^{-1}$ vitamin B5, 124.8 $mg \cdot l^{-1}$ ticarcillin disodium mixture, 30 $mg \cdot l^{-1}$ hygromycin, 1-naphthaleneacetic acid (final concentration 0.54 µM), 6-benzylaminopurine (8.88 µM), L-glutamine (342.14 µM), pH 5.8) to induce root formation at 16 h of light at 25°C. Plants with roots were transferred on a soil/sand mixture (1/1 (v/v)) for continuous growth. If not indicated otherwise, all chemicals purchased at Sigma-Aldrich.

Gene expression analysis

To confirm expression of *PMR4-GFP* and *GFP* in transformed Miscanthus lines, RNA was isolated from wild-type and the generated lines *35S:GFP* and *35S:PMR4-GFP* #1 and #2 lines using peqGOLD TriFast (Peqlab, Germany) according to the manufacturer's instructions. For complementary DNA (cDNA) synthesis, the Maxima First Strand cDNA Synthesis Kit (Thermo Scientific, USA) was used following the instructions of the manufacturer. The expression of *Actin* (Primer, 5'Act: 5'-ATGCACCAAGAGCTGTCTTC and 3'Act: 5'-GCTGGGCATTCAAAGGTTTC; primer sequences derived from *Miscanthus sinensis Actin* sequence (GenBank Acc. No. JN983213.1)) was used as reference for the expression of *PMR-GFP* (5'PMR4: 5'-ATCCAATACGCCCGTGAC and 3'GFP: GTGGCGGATCTTG AAGTTCAC) and *GFP* (5'GFP: 5'-ACGACGGCAACTACAAGAC and 3'GFP) in PCR reactions using the Q5 High-Fidelity DNA Polymerase (New England Biolabs, USA). Identity of amplified PCR products was confirmed by DNA sequencing.

1 Stitt, M., Lilley, R. M., Gerhardt, R. & Heldt, H. W. Metabolite levels in specific cells and subcellular compartments of plant leaves. *Methods Enzymol.* **174**, 518-552 (1989).

2 in *Lab FAQs - Find a Quick Solution* (eds U.W. Hoffmann-Rohrer & B. Kruchen) Ch. 5.1. Buffers, 153-166 (Roche Diagnostics GmbH, 2011).

3 Nataf, Y. *et al.* Cellodextrin and laminaribiose ABC transporters in *Clostridium thermocellum*. *J. Bacteriol.* **191**, 203-209 (2009).

4 Gietz, D., St Jean, A., Woods, R. A. & Schiestl, R. H. Improved method for high efficiency transformation of intact yeast cells. *Nucleic Acids Res.* **20**, 1425 (1992).